Title:

Endosomal-lysosomal organellar assembly (ELYSA) structures coordinate lysosomal degradation systems through mammalian oocyte-to-embryo transition

Authors:

Yuhkoh Satouh*[1], Takaki Tatebe[1], Isei Tanida[2], Junji Yamaguchi[2], Yasuo Uchiyama[2], Ken Sato*[1]

Affiliations:

1: Laboratory of Molecular Traffic, Institute for Molecular and Cellular Regulation, Gunma University, Maebashi, Japan.

2: Department of Cellular and Molecular Neuropathology, Juntendo University Graduate School of Medicine, Tokyo, Japan.

***Correspondence to:**

yuhkohs@gunma-u.ac.jp

sato-ken@gunma-u.ac.jp

Summary blurb

This study describes endosomal-lysosomal organellar assembly structures in mammalian oocytes, elucidating statistical alterations in their size, distribution, and correlation with lysosomal maturation.

Abstract:

Mouse oocytes undergo drastic changes in organellar composition and their activities during maturation from the germinal vesicle (GV) to meiosis II (MII) stage. After fertilization, the embryo degrades parts of the maternal components via lysosomal degradation systems, including autophagy and endocytosis, as zygotic gene expression begins during embryogenesis. Here, we demonstrate that endosomal-lysosomal organelles form large spherical assembly structures, termed ELYSAs, in mouse oocytes. ELYSAs are observed in GV oocytes, attaining sizes up to 7–8 μm in diameter in MII oocytes. ELYSAs comprise tubular-vesicular structures containing endosomes, lysosomes, autophagosome-like membranes in the outer layer, with cytosolic components contained within. The V1-subunit of vacuolar ATPase tends to localize to the periphery of ELYSAs in MII oocytes. After fertilization, the V1-subunit is recruited to immature endosomes and lysosomes as ELYSAs are gradually disassembled at the 2-cell stage, which leads to further acidification of endosomal-lysosomal organelles. These findings suggest that the ELYSAs maintain endosomal-lysosomal activity in a static state in oocytes for timely activation during early development.

Introduction:

Fertilization triggers the dynamic remodeling of cellular components via zygotic gene expression following the degradation of the cellular components of each maternal and paternal gamete. After fertilization, maternal cytosolic proteins and RNAs are selectively degraded by the ubiquitin-proteasome system (UPS)[1] and specific RNA degradation systems[2, 3], respectively. Treatment with a proteasome inhibitor or knockdown of the zygote-specific proteasome assembly chaperone gene inhibits cytokinesis in zygotes, suggesting an essential role for the UPS in early development[4, 5]. Membrane components derived from each gamete are degraded by the lysosomal degradation system via autophagy and endocytosis[6, 7]. In mice, autophagic activity is relatively low in meiosis II (MII) oocytes, whereas it is rapidly upregulated approximately 4 h after fertilization, and LC3-positive structures appear throughout the cytoplasm. Autophagic activity decreases slightly before and after the 2-cell stage but remains high from the 4- to 8-cell stage[8]. Loss of Atg5 causes embryonic lethality at the 4- to 8-cell stages, suggesting that autophagy is essential for early mouse development. In contrast, some maternal plasma membrane (PM) proteins are internalized from the PM at the late 2-cell stage and are selectively degraded by lysosomes[9]. Endocytosis inhibitors prevent cell division in 2-cell embryos, suggesting that endocytosis plays a pivotal role in early development[9, 10]. Although lysosomal degradation systems are drastically upregulated after fertilization, their regulation remains unknown.

In *Caenorhabditis elegans*, lysosomal activity in oocytes is upregulated by sperm-derived factors as the oocytes grow and mature. In this process, translational arrest of mRNA coding the V1-subunits of vacuolar ATPase in oocytes is released by the

stimulation of sperm-derived factors. Consequently, the V1-subunits are recruited to the V0-subunits in the lysosomal membrane, enhancing lysosomal acidification. This process is known as lysosomal switching[11]. In mouse embryos, LysoTracker staining analysis suggests that lysosomal acidification is prominent at the 2-cell stage but not in MII oocytes and zygotes[12], raising the possibility that lysosomal switching takes place during mouse embryogenesis.

In this study, we aimed to investigate the dynamics of the endolysosomal system during mouse oocyte maturation and embryogenesis. We found that endosomes and lysosomes assembled to form spherical structures in germinal vesicle (GV)-stage oocytes, which became larger as they matured into MII oocytes. Ultrastructural analysis showed that these structures were large spherical membrane assemblies, including endosomes, lysosomes, and tubulo-vesicular structures located in the periphery of the PM. We refer to this structure as the Endosomal-LYSosomal organellar Assembly (ELYSA). The ELYSA contains several cytosolic constituents. While ELYSAs are disassembled in late-stage zygotes, immature endosomes and lysosomes gradually appear in the cytoplasm of early 2-cell stage embryos. Live imaging analysis showed that the V1-subunit of V-ATPase is targeted to the endolysosomal membrane, resulting in further acidification of lysosomal compartments during embryogenesis. These findings suggest that the ELYSA maintains low endosomal and lysosomal activities and acts as a waiting place for endolysosomal organelles to undergo fertilization-triggered activation toward embryogenesis.

Results

Endosomes and lysosomes coordinately form giant structures in MII oocytes

To examine the localization of endosomes and lysosomes in mouse MII oocytes, early or late endosomes were stained with anti-RAB5 or RAB7 antibody, respectively, and their localization was compared with that of lysosomes stained with anti-LAMP1 antibody. Giant structures harboring lysosomes with early and late endosomes were detected (**Fig. 1A, Supplementary Fig. 1, Video 1**). Each giant structure in the MII oocytes was spherical, ellipsoidal, or concatenated with small spheres. These structures were located in the peripheral region just beneath the PM, excluding the metaphase plate region in proximity to the metaphase chromosomes. These structures were observed from the GV stage to the pronuclear-zygote (PN-zygote) stage but were mostly disassembled at the 2-cell stage. Dispersion and separation of RAB5 and LAMP1 signals after the first division indicated that these giant structures were transiently formed (**Fig. 1 B**).

Analyses of the number, size, and distribution of LAMP1-positive organelles were carried out by reconstituting three-dimensional objects using LAMP1-positive signals in immunocytochemically stained oocytes and embryos (**Supplementary Fig. 2**). Although the LAMP1 signals on the PM increased in the 2-cell stages, reconstitution of the objects was carried out only for the cytoplasmic fraction. The total number of the LAMP1-positive objects was highest at the GV stage, and it decreased toward the late 2-cell stage, with a significant difference compared to that in MII oocytes (**Fig. 2A**). Sorting of the objects based on their sizes (indicated with the diameters when converting the volume of each object to the corresponding sphere) revealed that the LAMP1-positive structures with

diameters of 0.2–0.8 μm, which were prominent in GV oocytes, significantly decreased toward the MII stage, while the number of giant LAMP1-positive structures with diameters of 3–7 μm decreased during the post-fertilization changes at the early and late 2-cell stage relative to that in MII (**Fig. 2B**). The transiently increased LAMP1-positive structures with 9–10 μm diameter at the early 2-cell stage were observed as concatenated spheres that gathered upon cellular division; concurrently, prominent signals on the PM appeared, especially at the cleavage furrow (**Fig. 2C, D**). The total volume of LAMP1-positive objects was highest in MII, and it decreased over the early and late 2-cell stages (**Fig. 2E**). LAMP1-positive structures with diameters of >3 μm were also observed in GV oocytes, but those larger than 5 μm in diameter were rarely detected, and the total volume of LAMP1-positive structures larger than 3 μm in diameter in MII oocytes accounted for 51.3% of the total volume. (**Fig. 2F**). The large population of the LAMP1-positive structures with diameters larger than 3 μm in MII transitioned to structures with diameters of 1–3 μm during the 2-cell stages, as indicated by the percentage of the volume of each object size relative to the total volume (**Fig. 2G**).

Furthermore, the analysis of object distribution for GV and MII oocytes indicated that MII oocytes had a greater number of LAMP1-positive structures with >4 μm diameter in the cellular periphery, whereas GV oocytes had a greater number of these structures in the cellular medial regions (**Fig. 2H, I**). These results suggest that the giant LAMP1-positive structures are enlarged and migrate to the cellular periphery during oocyte maturation.

Endosomes, lysosomes, and tubulo-vesicular structures form an ELYSA

To clarify the internal structure of this giant structure containing lysosomes and endosomes in the MII oocytes, we observed these in MII oocytes with in-resin correlative light and electron microscopy (CLEM) using immunological reaction (immune in-resin CLEM) with anti-RAB7 and -LAMP1 antibodies[13, 14]. RAB7- and LAMP1-signals were well detected even in the ultrathin section (100 nm thickness) of the Epon-embedded MII oocyte, fixed with the mixture of 4% paraformaldehyde and 0.025% glutaraldehyde (GA), which showed similar distribution as that shown in **Fig. 1** and **Supplementary Fig. 3**. Toluidine blue staining in adjacent ultrathin sections revealed that the RAB7/LAMP1-double positive structures in the fluorescence observation were also positive for toluidine blue, with interspaces were often found in the center of spheres (**Fig. 3A**). Confocal fluorescent images of the ultrathin sections clarified that RAB7-positive signals were frequently observed on the periphery of these LAMP1-positive signals. Electron microscopic analysis of the RAB7/LAMP1-double positive region in the ultrathin sections revealed that the RAB7/LAMP1-double positive structures are assemblies of tubulo-vesicular structures, with either vacuolated or filled interiors (**Fig. 3B**). The toluidine blue stain-positive structures were confirmed to match in size and peripheral distribution with those identified via RAB7/LAMP1 immunostaining, except for the metaphase plate, even under 2.5% GA conditions for precise ultrastructural observation (**Fig. 3C, Supplementary Fig. 4, Video 2**). Therefore, we examined the ultrastructural morphology of toluidine blue-positive giant structures in MII oocytes fixed with 2.5% GA. The results showed that tubular membrane vesicles with a short diameter of approximately

60.5 ± 15.9 nm assembled in the structure, with gaps in the cytoplasm of approximately 24.0 ± 6.7 nm. Some of the vesicles also harbored lysosome-like electron-dense contents, while others displayed multilamellar or multivesicular body-like structures, and mitochondria appeared to be absent (**Fig. 3D**). Based on these observations, we termed this membrane assembly the Endosomal-LYSosomal organellar Assembly (ELYSA).

An autophagosome marker, LC3, also accumulated in ELYSA

Decreased autophagic activity in MII oocytes is suggested by the fact that puncta formation of transgenically expressed GFP-LC3, an autophagosome marker, disappeared at the MII stage[8]. Since GFP fluorescence may be quenched under acidic conditions, we examined the localization of LC3 in GV and MII oocytes by immunostaining with an anti-LC3 antibody. We found that LC3 hardly formed puncta in the cytoplasm, but part of the LC3 signal overlapped with the ELYSA in both GV and MII oocytes (**Fig. 4A, B**), suggesting that LC3-positive membrane structures were also present in the ELYSA.

ELYSA enlargement and migration proceed actin dependently

The migration from the perinuclear (medial region) to the peripheral region during oocyte maturation (**Fig. 2H, I**) is similar to the redistribution of the endoplasmic reticulum (ER) and the formation of cortical ER clusters. Fitzharris et al. showed that the inhibition of actin cytoskeleton polymerization disturbs ER migration and cortical ER cluster formation[15]. Therefore, we added latrunculin A (LatA) or cytochalasin B (CCB) as inhibitors of actin polymerization, and nocodazole (Noco) as an inhibitor of microtubule formation, to

examine whether these affect ELYSA formation after *in vitro* maturation (IVM). While all the drugs inhibited polar body extrusion and metaphase plate formation as reported previously[15], co-immunostaining of LC3- or RAB5-antibody with LAMP1-antibody revealed their persistent colocalization in ELYSAs (**Fig. 5A, Supplementary Fig. 5**).

Analysis of LAMP1-positive organelles via three-dimensional object analysis indicated that the actin polymerization inhibitors increased the organelle number, particularly those with diameters in the range of 0.8–2 μm, but the tubulin inhibitor Noco did not have the same effect (**Fig. 5B, C**). The total volume of the objects was largely unchanged by the inhibitors. However, treatment with an actin polymerization inhibitor increased the percentage of total volume occupied by the structures with diameters of 1–2 μm, while conversely decreasing that of the structures with diameters of 4–7 μm that correspond to the enlarged ELYSAs (**Fig. 5D, E**). Further examination of the distribution of the LAMP1-positive structures in IVM oocytes indicated that only actin polymerization inhibitors reduced the number of objects larger than 4 μm in diameter at the cell periphery but not that in the cellular medial region (**Fig. 5F, G**).

V1 component of V-ATPase partially localizes to the periphery of ELISAs in oocytes

We studied the relationship between ELYSA formation and endosomal/lysosomal acidification in oocytes. V1A is a component of the V1 subunit of V-ATPase, which is associated with the outer lysosomal membrane and drives endosomal/lysosomal acidification. We used LAMP1-EGFP mRNA to observe ELYSA behaviors during oocyte maturation, with ATP6V1A-mCherry mRNA (V1A-mCherry: a core component of

V-ATPase fused with the mCherry marker) to further examine whether the V1 subunit is targeted to ELYSAs. The mRNAs were injected into GV oocytes, and the oocytes were applied to IVM.

Live-cell imaging of LAMP1-EGFP fluorescence captured the dynamics of LAMP1-positive organelles during oocyte maturation, notably demonstrating its stable expression after germinal vesicle breakdown (GVBD, 2–3 h after initiation of IVM), and revealed that the enlargement of ELYSAs larger than 5 μm in diameter occurred through the sequential assembly of smaller ELYSAs that constantly migrated and contacted each other (**Fig. 6A, Video 3**).

We then analyzed the localization of V1A-mCherry in the oocytes after IVM. Although V1A-mCherry signals were detected adjacent to LAMP1-positive organelles in deconvolved confocal images, they were largely distributed on the ELYSA surface and rarely observed within ELYSAs (**Fig. 6B, Video 4**).

Acidification of lysosomes is facilitated as ELYSA disassembly proceeds in embryos

We examined the relationship between ELYSA disappearance and the emergence of acidic membrane compartments during early development. LysoSensor probes exhibit increased fluorescence in a pH-dependent manner upon acidification and enable the semi-quantitative analysis of cellular acidic compartments, whereas LysoTracker probes exhibit non-pH-dependent fluorescence. We first co-stained oocytes and embryos at various stages with LysoTracker Red and LysoSensor Green (in the same medium drop). LysoTracker showed a pronounced puncta-like signal after the 2-cell stage, as previously

reported[12]. In contrast, the ELYSAs in GV and MII oocytes were clearly identified by LysoSensor, whereas LysoTracker only produced a very dim signal. Thus, the ratio of LysoTracker/LysoSensor fluorescent intensities in the cytoplasm of each stage embryo indicated that ELYSAs were present at a low ratio, while embryos at the 4-cell stage and beyond displayed small punctate signals with a higher ratio (**Fig. 7**). A comparison between LysoTracker and V1A-mCherry signals showed that these fluorescent signals colocalized well on small bright vesicles but not on the ELYSA, and both LysoTracker and V1A-mCherry puncta were reduced in embryos cultured in the presence of bafilomycin A_1, which inhibits the H^+ translocation of V-ATPase (**Supplementary Fig. 6**). This suggests that LysoTracker detects membrane compartment acidification, but it may not sufficiently capture this process within the ELYSA. In contrast, the results using LysoSensor suggest that lysosomes within the ELYSA were not completely neutralized and remained acidic at a lower level, even though V1A was difficult to localize.

To examine the spatiotemporal relationship between V1A localization and lysosomal acidification during embryogenesis, we injected V1A-mCherry mRNA to PN zygotes and cultured them in the presence of LysoSensor. It should be noted that stable detection of LysoSensor and V1A-mCherry fluorescence required 4–8 h. In this process, targeting of V1A to lysosomes was rarely observed until ELYSA disappearance or disassembly throughout the PN-zygote stage, but the targeting was rapidly enhanced in the early 2-cell embryo stage. LysoSensor-positive punctate structures, where V1A-mCherry accumulated, increased in number during the transition from early to late 2-cell stage, indicating that lysosomal acidification is promoted after ELYSA disappearance (**Fig. 8,**

Video 5).

Low-level cathepsin-dependent proteolytic activity was maintained in ELYSA

Cathepsins are mainly responsible for the proteolytic activity in lysosomes. We visualized the proteolytic activity of cathepsin B, the expression of which has been confirmed in mouse embryos[12]. Mouse oocytes and embryos at various stages were simultaneously collected and stained with Magic Red cathepsin B staining solution to examine their relationship with the ELYSA. Magic Red staining showed that proteolytic activity was detected not only in the small, isolated membrane structures (mature lysosomes) but also in the ELYSA in the GV and MII oocytes, whereas small punctate structures were predominantly stained in other stages (**Supplementary Fig. 7, Fig. 9A**). The intensity plots of LysoSensor and Magic Red fluorescence revealed that the proteolytic activity indicated by the Magic Red signal in the ELYSA was not as strong as that in isolated punctate structures (lysosomes) in the GV and MII oocytes (**Fig. 9B**).

Discussion:

In this study, we identified a large spherical structure, the ELYSA, consisting of endosomes, lysosomes, LC3-positive vesicles, and various vesicular-tubular structures in mouse oocytes . Small ELYSAs are formed in GV oocytes and become larger (3 to 7 μm in diameter) through assembly, migrating to the cellular periphery, in an actin-dependent manner during oocyte maturation and occupy more than half the volume of the LAMP1-positive fraction in MII oocytes. After fertilization, as ELYSAs gradually

disassemble in zygotes, punctate structures positive for either RAB5- or LAMP1-signal alone appear in the cytoplasm of embryos at the early 2-cell stage. The V1-subunit of V-ATPase is targeted to these structures, leading to further acidification of the endosomal/lysosomal compartments. These results suggest that the ELYSA functions as a reservoir that accumulates endosomal and lysosomal compartments in the periphery of the cell cortex and maintains their activities in a static state until embryogenesis following fertilization.

We have studied the dynamics and activity of endosomes and lysosomes in mouse oocytes and embryo and have found that some oocyte PM proteins are internalized from the PM at the late 2-cell stage and are selectively degraded in lysosomes[9]. In this process, we noted that lysosomes were not well stained by LysoTracker until the early 2-cell stage, but their signals became stronger from the late 2-cell stage, suggesting the existence of a mechanism underlying developmentally regulated endosomal/lysosomal activation during embryogenesis[9, 12]. Notably, ELYSAs were stained with toluidine blue and LysoSensor, suggesting that these structures were acidified to some extent (**Fig. 3, 7**). In addition, Magic Red, which reflects cathepsin B activity, weakly stained ELYSAs (**Fig. 9**). These observations indicate that lysosomes in ELYSAs have some activity, albeit at low levels. Mouse oocytes accumulate several maternal constituents, including proteins, lipids, and mRNA, and grow to approximately 75 μm in diameter. In addition, oocytes must remain at the GV and MII stages for an extended period to maintain their quality until fertilization. In such situations, lysosomal degradation activity may be suppressed to a relatively low level by the ELYSA, whereas nutrient uptake, storage, and protein synthesis are predominantly

upregulated in growing oocytes. Furthermore, we found that the V1-subunits were largely detected on the periphery of ELYSAs but not in their interior in oocytes (**Fig. 6**). Thus, it is possible that ELYSA formation prevents V1-subunits from targeting the lysosomal membrane inside the ELYSA.

Ultrastructural analysis revealed that the ELYSA consists of outer and inner membrane assembly layers that contain several endosomes and lysosomes, respectively (**Fig. 1, 3**). Upon disassembly of the ELYSA, endosomes in the outer layer and lysosomes in the inner layer are expected to be released from the ELISA earlier and later, respectively. This may explain the time lag between fertilization and lysosomal acidification beginning at the early-2-cell stage. Since the ELYSA appears to contain cytosolic constituents, it may accommodate some cytosolic constituents as a capsule to provide nutrition or signaling factors for development.

ELYSAs were gradually distributed from the perinuclear region to the periphery of the oocyte cell cortex, except in the MII cell plate, from the GV to the MII stage (**Fig. 1, 2**). This movement is reminiscent of that of the ER and cortical ER clusters, whose distribution is regulated by the actomyosin system[15]. In fact, the treatment of actin cytoskeleton polymerization inhibitors, but not a tubulin polymerization inhibitor, prevented the redistribution of ELYSAs from the cell cortex to the cytoplasm in oocytes (**Fig. 5**). The former treatment increased the number of small LAMP1-positive organelles but reduced the size of ELYSAs in oocytes (**Fig. 5**). These results suggest that actin cytoskeleton is involved in the assembly of smaller (<2 μm in diameter) LAMP1-positive organelles for the enlargement of ELYSAs and also in the redistribution of ELYSAs to the cell periphery.

Our detailed imaging analysis showed that lysosomal acidification is promoted by the accumulation of the V1-subunits on lysosomes during ELYSA disassembly in late zygotes and is further facilitated from the 2- to 4-cell stage and is enhanced after the morula stage (**Fig. 8, Supplementary Fig.6**). These findings suggest that lysosomal acidification and maturation are linked to the ELYSA disassembly. Notably, minor and major zygotic gene activation in mouse embryos occur at the 1- and 2-cell stages, respectively, implying that lysosomal degradation of maternal components is coupled with zygotic gene expression to promote embryogenesis[16]. Fertilization appears to trigger ELYSA disassembly, but the downstream signaling pathways remain to be identified and warrant further research.

Very recently, after sharing this ELYSA paper as a preprint in 2023[17], Zaffagnini et al. reported the endolysosomal vesicular assemblies (ELVAs), which resemble with ELYSAs, in mouse oocytes[18]. Consistencies between the ELVA and ELYSA in their contents and actin-dependent dynamics during oocyte maturation/embryogenesis strongly suggests that ELYSAs and ELVAs are identical structures[18], assuring the solidity of these findings in this paper. Zaffagnini et al. also observed the accumulation of proteasomes and ubiquitinated proteins in ELVAs and demonstrated that the depletion of a RUN and FYVE domain-containing protein 1 (RUFY1) protein from oocytes by the Trim-Away method causes disappearance of ELVAs, suggesting that RUFY1 is involved in the ELVA assembly. Analysis of *Rufy1*-knockout ELVA/ELYSA free oocytes is awaited to elucidate the physiological role of ELVAs or probably ELYSAs. They also suggested that ELVAs sequester and degrade specific proteins that is known to be aggregate and cause diseases,

326 including proto-oncogene receptor tyrosine kinase KIT, upon oocyte maturation[18].
327 Complementally to their findings, our study revealed that the recruitment of the V1-subunit
328 is limited on ELYSAs in oocytes but enhanced on the isolated LAMP1-positive vesicles
329 after late 2-cell stage. These findings support a hypothesis that ELYSA has a multimodal
330 function, keeping endosomal and lysosomal compartments at a relatively static state and
331 supplying these membrane compartments as a reservoir for embryogenesis.

332 Inhibition of lysosomal acidification by bafilomycin A_1 treatment arrests
333 embryogenesis at the 4–8-cell stage, while inhibition of cathepsin activity using a mixture
334 of E64d and pepstatin A blocks embryogenesis at the 8-cell or morula stage[12]. In contrast,
335 the inhibition of endocytosis by Pitstop2 treatment causes arrest at the 2-cell stage[9]. These
336 differences may imply that at the 2-cell stage, the endocytic activity is more important than
337 the lysosomal degradation activity, which is essential at later stages. However, insights
338 from this study shed light on the correlation between increased endocytic/autophagic
339 activity and lysosomal maturation through ELYSA disassembly and the potential
340 significance of minor lysosomal maturation in the early phase of embryogenesis.

341 The relationship between such endocytic/autophagic activities in early-stage
342 embryos and the embryonic developmental potential have been recently studied. Using
343 GFP-LC3 as an indicator of autophagic activity, Tsukamoto et al. found that aged oocytes
344 from 14- to 15-month-old mice had lower autophagic activity than those from younger
345 mice, probably due to decreased lysosomal activity. Females transplanted with embryos
346 with high autophagic activity at the 4-cell stage have a significantly higher litter size ratio
347 than that of control females[19]. Analysis of ELYSA formation and disassembly in aged

oocytes and embryos may be a useful tool for determining oocyte quality by examining appropriate regulation of endosomal/lysosomal activities.

Methods:

Animal experiments and strains

Neither randomization nor blinding was used for animal selection (8–16-week-old). All experimental protocols involving animals were approved and performed in accordance with the guidelines of the Animal Care and Experimentation Committee of Gunma University (Approval No. 22-076). Hybrid B6D2F1 mice were purchased from the Japan SLC (Hamamatsu, Japan)

Antibodies and inhibitors

The following primary antibodies were used: rabbit monoclonal anti-RAB5 (C8B1; 3547; Cell Signaling Technology, Danvers, MA, USA), rabbit monoclonal anti-RAB7 (D95F2; 9367; Cell Signaling Technology), rat monoclonal anti-mouse LAMP1 (1D4B; sc-19992; Santa Cruz Biotechnology, Dallas, TX, USA), and mouse monoclonal anti-rat LC3 (Clones 4E12; M152-3; Medical and Biological Laboratories, Tokyo, Japan). The following secondary antibodies were used: goat anti-rabbit IgG (H+L) conjugated with Alexa Fluor 555 (A-21428; Thermo Fisher Scientific, Waltham, MA, USA), goat anti-rat IgG (H+L) cross-adsorbed secondary antibody conjugated with Alexa Fluor 488 and 647 (A-11006 and A-21247, respectively; Thermo Fisher Scientific), and goat anti-mouse IgG (H+L) cross-adsorbed secondary antibody conjugated with Alexa Fluor 546 (A-11030; Thermo

Fisher Scientific). The following inhibitors or solutions were used for IVM or embryonic culture assays: dimethyl sulfoxide (DMSO) (13406-55; Nacalai Tesque, Kyoto, Japan); latrunculin A actin polymerization inhibitor that binds to monomer actin (428021; Sigma-Aldrich, St. Louis, MO, USA); cytochalasin B, an actin polymerization inhibitor that binds to the plus-end of polymerized actin (C6762; Sigma-Aldrich); and nocodazole, a tubulin polymerization inhibitor that binds to β-tubulin (M1404; Sigma-Aldrich). Stock solutions of latrunculin A, cytochalasin B, or nocodazole were prepared by solubilizing each in DMSO at 200× concentration for the assays. Bafilomycin A_1 was dissolved in DMSO (L266; Dojindo, Kumamoto, Japan) at a final concentration of 25 nM.

Oocyte preparation

GV oocytes were collected from the ovaries of female mice 46 h after injection with pregnant mare serum gonadotropin or an anti-inhibin antibody (CARD HyperOva; Kyudo, Kumamoto, Japan). Antral follicles were suspended in 30 μL of FHM medium drops (Sigma-Aldrich) covered with liquid paraffin (Nacalai Tesque), punctured using 26G needles (Terumo, Tokyo, Japan), and the GV oocytes were collected using a glass needle with a mouth pipette. MII oocytes were collected from the oviducts of female mice 13 h after injection with CARD HyperOva and 7.5 IU human chorionic gonadotropin (hCG; ASKA Pharmaceutical, Tokyo, Japan) 48 h apart. The oviductal wall was punctured using a 26G needle to collect cumulus-oocyte complexes in 20 μL potassium simplex optimization medium (KSOM; Kyudo) drops covered with liquid paraffin.

DNA vector construction and mRNA synthesis

Complementary DNA for mouse *Lamp1* (accession number NM_001317353) or *Atp6v1a* (accession number NM_001358204) was amplified using PCR with High-fidelity Taq Polymerase, KOD FX Neo (Toyobo, Osaka, Japan), and a mouse ovary cDNA library as a template (Genostaff, Tokyo, Japan). The amplicon was then subcloned into the entry vector pDONR221, and transferred into the destination vectors pDEST-CMV-C-EGFP (#122844; for *Lamp1*; Addgene, Watertown, MA, USA) or pDest-mCherry-N1 (#31907; for *Atp6v1a*; Addgene) using Gateway recombination cloning technology. The following primer combinations were used for cloning: 5′-GCGCACAAGTTTGTACAAAAAAGCAGGCTGCCACCATGGCGGCCCCCGGCG-3′ and 5′-GCGCACCACTTTGTACAAGAAAGCTGGGTTGTCTTCAAGGCTACGGAATG-3′ (for *Lamp1*), or 5′-GCGCACCACTTTGTACAAGAAAGCTGGGTTGATGGTCTGATAGCCGGCGTGACT-3′ and 5′-GCGCACCACTTTGTACAAGAAAGCTGGGTTGTCTTCAAGGCTACGGAATG-3′ (for *Atp6v1a*). The cDNA encoding *Lamp1-EGFP* or *Atp6v1a-mCherry* were amplified using the following primer combinations: 5′-CGCAAATGGGCGGTAGGCGTG-3′ and 5′-TCCAGCAGGACCATGTGATCGC-3′ (for *Lamp1-EGFP*), or 5′-CGCAAATGGGCGGTAGGCGTG-3′ and 5′-TTGGTCACCTTCAGCTTGG-3′ (for *Atp6v1a-mCherry*). RNA synthesis using each PCR amplicon as a template, poly-A tail addition, and mRNA purification were performed, using an mMESSAGE mMACHINE T7

Ultra kit (Thermo Fisher Scientific) and MEGAclear transcription clean-up kit (Thermo Fisher Scientific), according to the manufacturer's protocols. Synthesized mRNAs were dissolved in RNase-free demineralized water at a concentration of 400 ng/μL and frozen in aliquots until use.

In vitro maturation, fertilization, and embryonic culture

IVM for the GV oocytes was conducted by washing the oocytes twice and culturing in alpha-modified Eagle's minimum essential medium (Thermo Fisher Scientific) containing 5% (vol/vol) fetal bovine serum (FBS), 0.1 of IU/mL follicle-stimulating hormone (MSD, Tokyo, Japan), 1.2 IU/mL of hCG (ASKA Pharmaceutical), and 4 ng/mL of epidermal growth factor (Thermo Fisher Scientific) for 17 h at 37 °C under a 5% CO_2 atmosphere[20]. For *in vitro* fertilization, spermatozoa from a B6D2F1 epididymis were pre-incubated in a 100-μL modified human tubal fluid medium (Kyudo) drop covered with liquid paraffin and inseminated at a sperm concentration of 1.5×10^5 per mL for 1.5 h. Excess spermatozoa were washed out, and the oocytes were incubated in a 20-μL KSOM drop (Kyudo) for further development. IVM assays using latrunculin A and cytochalasin B were performed by transferring oocytes to medium drops containing each inhibitor or DMSO 4 h after the start of IVM (waiting for the completion of GVBD), as previously reported[15]. IVM media containing DMSO, latrunculin A, or cytochalasin B was prepared by diluting the stock solution (1:400), and the final concentration of the inhibitors was 10 μM. The embryonic culture assay using bafilomycin A_1 was conducted by transferring the PN-zygote into a 20-μL drop of KSOM containing 25 nM bafilomycin A_1 covered with liquid paraffin at 6 h

post-fertilization (hpf). Embryos were transferred at 24, 48, and 72 hpf to freshly prepared KSOM containing bafilomycin A_1.

Immunostaining

Immunostaining of oocytes or embryos was performed as previously described[9]. Oocytes or embryos were cultured to the indicated stages and fixed in 4% paraformaldehyde (PFA; Nacalai Tesque) in phosphate-buffered saline (PBS) containing 0.1 mg/mL polyvinyl alcohol (PVA; Sigma-Aldrich) (PVA/PBS) for 15 min at 25–27 °C. After fixation, the cells were permeabilized with PVA/PBS containing 0.1% Triton X-100 (Sigma-Aldrich) for 30 min at 25–27 °C and washed three times with PVA/PBS. After blocking with 10% FBS (Thermo Fisher Scientific) in PBS for 1 h at room temperature, the cells were incubated with the aforementioned primary antibodies (1:100 for all) overnight at 4 °C. Next, the cells were washed three times in PVA/PBS, and incubated with anti-mouse, rat, or rabbit IgG secondary antibodies coupled with Alexa Fluor 488, 555, or 564 (1:200 for all; Thermo Fisher Scientific) at 25–27 °C for 2–4 h. Thereafter, the cells were incubated with PVA/PBS containing 10 μg/mL Hoechst 33342 (Dojindo) for 10 min and washed with fresh PVA/PBS a few times. Subsequently, control and nonspecific staining were performed by processing oocytes and embryos in the absence of primary antibodies. The oocytes and embryos were imaged in PVA/PBS microdrops in 35-mm glass-bottomed dishes (MatTek Corporation, Ashland, MA, USA). For each position, confocal images at 81 *z*-axis planes with 1-μm increments were acquired on an IX-71 inverted microscope (Olympus Corporation, Tokyo, Japan) equipped with a CSU W-1 confocal scanner unit (Yokogawa Electric Corporation)

using a 60× silicone immersion lens UPLSAPO60XS (Olympus Corporation).

LysoTracker/LysoSensor staining of oocytes and generation of ratio images

Acidic organelles in the oocytes were visualized using LysoTracker Red DND-99 and LysoSensor Green DND-189 (Thermo Fisher Scientific) according to the manufacturer's instructions. Briefly, the oocytes or embryos at target stages for one experimental round were obtained simultaneously and incubated in a large drop of reaction mixture (KSOM containing 1/10,000 Magic Red stock solution dissolved in DMSO and 1/1,000 LysoSensor Green DND-189 stock solution dissolved in DMSO) for 30 min at 37 °C under 5% CO_2 in a humidified atmosphere in liquid paraffin in a 35-mm glass-bottom dish (MatTek Corporation). Subsequently, confocal images at 41 *z*-axis planes with 2-μm increments were obtained using a CSU W-1 spinning disk confocal microscope with a 30× silicone immersion lens UPLSAPO30XS (Olympus Corporation). Acquisition conditions for fluorescence excited by 470-nm (LysoSensor) and 555-nm (LysoTracker) lasers were determined in preliminary experiments to be almost 1:1 intensities between the two wavelengths for cytosolic punctate structures in the 2-cell embryo. Further generation of ratio images for LysoTracker/LysoSensor fluorescence were carried out using Fiji software[21]. Averaged intensity projection was carried out, determining background intensity of each field by subtracting the averaged intensities of four cellular blank regions from the whole image. Then, 32-bit ratio images for LysoTracker/LysoSensor fluorescence of cytosolic regions were generated by processing images with "Math/Divide" function in Fiji, and "fire" look up table images were converted to RGB images.

480

481 ***Magic Red/LysoSensor staining***

482 Intracellular cathepsin activity was assayed in oocytes or embryos using Magic Red
483 Cathepsin B or Cathepsin L detection kits (ImmunoChemistry Technologies LLC, Davies,
484 CA, USA) according to the manufacturer's instructions. Briefly, the oocytes or embryos at
485 target stages for one experimental round were obtained simultaneously and incubated in a
486 large drop of reaction mixture (KSOM containing 1/250 Magic Red stock solution
487 dissolved in DMSO and 1/1,000 LysoSensor Green DND-189 stock solution dissolved in
488 DMSO) for 25 min at 37 °C under 5% CO_2 in a humidified atmosphere in liquid paraffin in
489 a 35-mm glass-bottom dish (MatTek Corporation). Thereafter, Hoechst 33342 (10 μg/mL)
490 was added to the drop to a final concentration of 10 μg/mL, and incubated for 5 min.
491 Subsequently, oocytes or embryos at the same stage were collected, and confocal images at
492 41 *z*-axis planes with 2-μm increments for both 470-nm (LysoSensor) and 555-nm (Magic
493 Red) lasers were obtained on a CSU W-1 spinning disk confocal microscopy using a 30×
494 silicone immersion lens UPLSAPO30XS (Olympus Corporation).

495

496 ***In-resin CLEM and electron microscopy***

497 In-resin CLEM was performed as previously described with some modifications[13, 14].
498 Briefly, oocytes were fixed in 4% PFA and 0.025% glutaraldehyde (GA). After
499 permeabilization with 50 μg/mL digitonin (Nacalai Tesque) and 0.02% Triton X-100,
500 oocytes were washed with PVA/PBS three times and incubated with PBS containing 10%
501 (w/v) FBS (Thermo Fisher Scientific) for 1 h at room temperature. Thereafter, oocytes were

incubated with PVA/PBS containing primary antibody overnight at 4 °C. After incubation with a secondary antibody in PVA/PBS for 2 h, oocytes were fixed in 4% PFA and 2.5% GA, embedded in 1.5% agarose, stained with osmium tetroxide, dehydrated with graded ethanol solutions (QY1), and embedded in epoxy resin (Oken Shoji, Tokyo, Japan). Ultrathin sections of Epon-embedded oocytes (100-nm thickness) were prepared using a Leica UC6 ultramicrotome (Leica, Nussloch, Germany) and placed on glass coverslips. Subsequently, fluorescence microscopy images of the sections were obtained using a Nikon A1RHD25 confocal laser scanning microscope with a NIS-Elements software (Nikon, Tokyo, Japan). Electron microscopic images were observed using a Helios Nanolab 660 FIB-SEM instrument (FEI Company, Hillsboro, USA).

For conventional electron microscopy, the oocytes were fixed in the presence of 2% PFA and 2.5% GA and stained with osmium tetroxide. After dehydration with ethanol, the oocytes were embedded in epoxy resin, as described above. Sections were cut at a thickness of 100 nm using a UC6 ultramicrotome, mounted on glass coverslips, stained with uranyl acetate and lead citrate, and observed under a Regulus8240 scanning electron microscope (Hitachi High-Tech Corporation, Tokyo, Japan).

Serial semi-thin sections and 3D reconstruction of toluidine blue-positive structures

Serial semi-thin sections were cut at a thickness of 300 nm using a UC6 ultramicrotome and mounted on glass slides. Next, the sections were stained with 1% toluidine blue/0.1 M PB, and images were obtained using a BX50 light microscope (Olympus Corporation). Serial toluidine blue-stained images were aligned using FIJI (National Institutes of Health,

MD, USA) with plugin-linear stack alignment using SIFT (LSAS), and 3D reconstruction was performed using Amira software (Thermo Fisher Scientific).

Microinjection into the oocytes

Microinjection of mRNA into GV oocytes was performed as previously described[22, 23]. Briefly, antral follicles were harvested in FHM medium containing 250 μM of dbcAMP using 26G needles (Terumo). After dissociating the cumulus cells by pipetting, the oocytes were transferred to medium supplemented with 250 μM of dbcAMP and 10 μM of cytochalasin B (Sigma-Aldrich). Thereafter, mRNA injection into the oocytes was performed using a piezo-micromanipulator (Primetech, Tokyo, Japan) with a glass capillary needle. The mRNA concentrations were 50 and 100 ng/μL for *V1A-mCherry* and *Lamp1-EGFP*, respectively. The oocytes were washed three times and used for IVM. Microinjection of mRNA into zygote stage embryo (at 3–4 hpf) was carried out as previously described[9]. The concentration of mRNA was the same as that in the GV oocytes.

Time-lapse confocal imaging of oocytes/embryos

Low-invasive confocal fluorescence imaging of oocytes/embryos was performed as previously described[24, 25, 26] with slight modifications. Briefly, on an inverted microscope IX-71 (Olympus Corporation) equipped with a CSU W-1 confocal scanner unit (Yokogawa Electric Corporation), an incubation chamber (Tokai Hit, Fujinomiya, Japan) was set at 37 °C on the microscope stage, with a gas mixture of 5% CO_2 introduced into the chamber at 150 mL/min. Oocytes/embryos were placed in 8 μL of IVM medium or KSOM drops

covered with liquid paraffin (Nacalai Tesque) in 35-mm glass-bottomed dishes (MatTek Corporation). Subsequently, confocal images at 41 *z*-axis planes with 2-μm increments for excitation lasers of 470- and 555-nm from an LDI-7 Laser Diode Illuminator (89North, Williston, VT, USA) were obtained every 30 or 60 min during IVM or embryonic culture observation, respectively, through optimized band-pass filters using 30× silicone immersion lens UPLSAPO30XS (Olympus Corporation).

Three-dimensional object analysis

Series of confocal images with 81 z-axis planes with 1-μm increments for LAMP1 immunostaining were used for 3D object analysis. Fields to analyze were cropped for each oocyte/embryo, and the upper and lower end of LAMP1 fluorescent signals in the cytosol were examined to determine the center plane (middle height) of the cell. The cellular region in the center plane was used for masking and determination of the geometric center (as a 3D center) of each oocyte. Deletion of the signals from the polar body or zona pellucida was carried out manually. Objects were profiled using the 3D object counter plugin[27] of Fiji software[21], to measure the number, volume, geometric center of each object, and mean distance from the geometrical center of the object to its surface. Thresholding was carried out after background subtraction using the Fiji software, manually applying intensities of 600–1200 as threshold to recognize objects separately. Signals on PM were eliminated both via size filtering (0–5000 μm^3) of the 3D object counter plugin and manual erasing. The distal distance of each object from the 3D center of the oocyte was used for distribution analysis to avoid underestimation of the distance of large ELYSA. This was calculated by

adding the distance from the 3D center of the oocyte to the geometric center of each object and the mean distance from the geometrical center of the object to its surface. Distance calculation and generation of bar graphs were carried out using Excel 2016 software (Microsoft, Redmond, WA, USA).

Analysis of microscopic images and movies

Analysis of the acquired images, including the generation of a line plot of intensity, adjustment of intensity, and generation of montage images at a uniform intensity, was performed using Fiji software[21]. To enhance the images, a Gaussian Blur filter (at a sigma radius of 1) and auto-adjustment of the intensity were applied to the stack of images. To adjust the intensity, auto-adjustment of the intensity was applied to each image. The movies were concatenated using Premiere Pro software (Adobe, San Jose, CA, USA).

Statistics and reproducibility

Sample sizes were estimated based on previous studies using similar experiments, and results from preliminary experiments were examined to ensure statistical power more than 0.8 using statistical power analysis in the G*Power software[28]. Statistical analyses and generation of dot plot graphs were performed using Graph-Pad Prism 8 (GraphPad Software, Boston, MA, USA). The significance of difference among groups were compared using one-way ANOVA. The experimenters were not blinded because of a limitation in the availability of experienced personnel.

Data availability:

The data supporting the findings of this study are available from the corresponding authors upon request.

Materials availability statement:

The materials supporting the findings of this manuscript are available from the corresponding authors upon reasonable request.

Acknowledgments:

We would like to thank Editage (www.editage.jp) for English language editing.

Funding:

This study was supported by the Japan Society for the Promotion of Science KAKENHI (Grant Numbers 19H05711 and 20H00466 to K. Sato, 21H02435, 22H02872, and 22H04652 to I. Tanida, and 20K22744 to J. Yamaguchi), the Mochida Memorial Foundation for Medical and Pharmaceutical Research, Takeda Science Foundation (Grant Number 2022093867), and The Cell Science Research Foundation to Y. Satouh. This work was partly supported by the Project for Elucidating and Controlling Mechanisms of Aging and Longevity from the Japan Agency for Medical Research and Development (AMED 21gm5010003 to Y. Uchiyama., 22gm1710001 s0201 and 23gm1710001s0202 to I. Tanida) and by the MEXT-supported Program for the Strategic Research Foundation at Private Universities (to Y. Uchiyama), and the Center of Genomic and Regeneration Medicine,

Juntendo University Graduate School of Medicine (to Y. Uchiyama and I. Tanida).This work was partly supported by the joint research program of the Institute for Molecular and Cellular Regulation, Gunma University (24014 to I. Tanida and K. Sato).

Competing interests:

No competing interests declared.

Author contributions:

Y.S. and K.S. established the essential research concepts for this study. Y.S. and T.T. performed immunostaining and assays using mouse oocytes/embryos. I. T., J. Y., and Y. U. performed the CLEM experiments and analyses. Y. S. and K. S. prepared the manuscript.

References:

1. Verlhac MH, Terret ME, Pintard L. Control of the oocyte-to-embryo transition by the ubiquitin-proteolytic system in mouse and *C. elegans*. *Curr Opin Cell Biol* **22**, 758-763 (2010).

2. Jiang ZY, Fan HY. Five questions toward mRNA degradation in oocytes and preimplantation embryos: when, who, to whom, how, and why? *Biol Reprod* **107**, 62-75 (2022).

3. Schier AF. The maternal-zygotic transition: death and birth of RNAs. *Science* **316**,

406-407 (2007).

4. Shin SW, *et al.* Mouse zygote-specific proteasome assembly chaperone important for maternal-to-zygotic transition. *Biol Open* **2**, 170-182 (2013).

5. Shin SW, *et al.* Inhibition of the ubiquitin-proteasome system leads to delay of the onset of ZGA gene expression. *J Reprod Dev* **56**, 655-663 (2010).

6. Sato K. Multiple roles of endocytosis and autophagy in intracellular remodeling during oocyte-to-embryo transition. *Proc Jpn Acad Ser B Phys Biol Sci* **98**, 207-221 (2022).

7. Birgisdottir AB, Johansen T. Autophagy and endocytosis - interconnections and interdependencies. *J Cell Sci* **133**, (2020).

8. Tsukamoto S, Kuma A, Murakami M, Kishi C, Yamamoto A, Mizushima N. Autophagy is essential for preimplantation development of mouse embryos. *Science* **321**, 117-120 (2008).

9. Morita A, Satouh Y, Kosako H, Kobayashi H, Iwase A, Sato K. Clathrin-mediated endocytosis is essential for the selective degradation of maternal membrane proteins and preimplantation development. *Development* **148**, dev199461 (2021).

10. Satouh Y, Sato K. Reorganization, specialization, and degradation of oocyte maternal components for early development. *Reprod Med Biol* **22**, e12505 (2023).

11. Bohnert KA, Kenyon C. A lysosomal switch triggers proteostasis renewal in the immortal *C. elegans* germ lineage. *Nature* **551**, 629-633 (2017).

12. Tsukamoto S, *et al.* Functional analysis of lysosomes during mouse preimplantation embryo development. *J Reprod Dev* **59**, 33-39 (2013).

13. Tanida I, Yamaguchi J, Suzuki C, Kakuta S, Uchiyama Y. Application of immuno- and affinity labeling with fluorescent dyes to in-resin CLEM of Epon-embedded cells. *Heliyon* **9**, e17394 (2023).

14. Mitsui S, Yamaguchi J, Suzuki C, Uchiyama Y, Tanida I. TUNEL-positive structures in activated microglia and SQSTM1/p62-positive structures in activated astrocytes in the neurodegenerative brain of a CLN10 mouse model. *Glia* **71**, 2753-2769 (2023).

15. FitzHarris G, Marangos P, Carroll J. Changes in endoplasmic reticulum structure during mouse oocyte maturation are controlled by the cytoskeleton and cytoplasmic dynein. *Dev Biol* **305**, 133-144 (2007).

16. Schulz KN, Harrison MM. Mechanisms regulating zygotic genome activation. *Nat Rev Genet* **20**, 221-234 (2019).

17. Satouh Y, *et al.* Endosomal-lysosomal organellar assembly (ELYSA) structures coordinate lysosomal degradation systems through mammalian oocyte-to-embryo transition. [**Preprint**] *bioRxiv* 2023.12. 29.573616 (2023) https://doi.org/10.1101/2023.12.29.573616

18. Zaffagnini G, *et al.* Mouse oocytes sequester aggregated proteins in degradative super-organelles. *Cell* **187**, 1109-1126 e1121 (2024).

19. Tsukamoto S, *et al.* Fluorescence-based visualization of autophagic activity predicts mouse embryo viability. *Sci Rep* **4**, 4533 (2014).

20. Morohaku K, *et al.* Complete in vitro generation of fertile oocytes from mouse primordial germ cells. *Proc Natl Acad Sci U S A* **113**, 9021-9026 (2016).

21. Schindelin J, *et al.* Fiji: an open-source platform for biological-image analysis. *Nat Methods* **9**, 676-682 (2012).

22. Umeda R, *et al.* Structural insights into tetraspanin CD9 function. *Nat Commun* **11**,

1606 (2020).

23. Kato K, *et al.* Structural and functional insights into IZUMO1 recognition by JUNO in mammalian fertilization. *Nat Commun* **7**, 12198 (2016).

24. Nozawa K, Satouh Y, Fujimoto T, Oji A, Ikawa M. Sperm-borne phospholipase C zeta-1 ensures monospermic fertilization in mice. *Sci Rep* **8**, 1315 (2018).

25. Satouh Y, Nozawa K, Yamagata K, Fujimoto T, Ikawa M. Viable offspring after imaging of Ca^{2+} oscillations and visualization of the cortical reaction in mouse eggs. *Biol Reprod* **96**, 563-575 (2017).

26. Satouh Y, Inoue N, Ikawa M, Okabe M. Visualization of the moment of mouse sperm-egg fusion and dynamic localization of IZUMO1. *J Cell Sci* **125**, 4985-4990 (2012).

27. Bolte S, Cordelieres FP. A guided tour into subcellular colocalization analysis in light microscopy. *J Microsc* **224**, 213-232 (2006).

28. Faul F, Erdfelder E, Lang AG, Buchner A. G*Power 3: a flexible statistical power analysis program for the social, behavioral, and biomedical sciences. *Behav Res Methods* **39**, 175-191 (2007).

Figure legends:

Fig. 1. Endosomes and lysosomes form giant structures in the periphery of the oocyte plasma membrane.

(A) Meiosis II (MII) oocytes were fixed and co-stained with anti-RAB5 and anti-LAMP1 antibodies. The schematic diagram indicates the location of oocyte chromosomes and metaphase plate in the MII oocytes. Maximum intensity projection of confocal images at an axial scan range of 80 μm is shown as Z-projection images. Arrowheads indicate the positions of oocyte chromosomes. Magnified regions (right) are indicated by yellow boxes. (B) Embryos at different stages were fixed and co-stained with anti-RAB5 and anti-LAMP1 antibodies. Hour(s) post-fertilization is indicated as hpf. DNA was stained with Hoechst 33342.

Fig. 2. Endosomes and lysosomes form giant structures in the periphery of the MII oocyte PM

Germinal vesicle (GV) oocyte, MII oocyte, early 2-cell (E2C: 24 hpf), and late 2-cell (L2C: 40 hpf) embryos were fixed and stained with anti-LAMP1 antibody. Reconstituted three-dimensional objects for the LAMP1-positive organelles in 9 to 10 oocytes for each stage from more than three independent experiments were further analyzed for number, size and distribution. (A) Averaged total object number per oocyte/embryo. (B) Numbers of the objects sorted by size (indicated by the diameters of spheres calculated from volumes) with an inset indicating an enlarged graph of the dotted region. (C) Ratios of (B) to the average

of MII oocyte, (D) A single confocal section image for E2C embryos which have transient and concatenated objects upon cellular division (arrowhead) and a prominent signal on the PM of cleavage furrow (dotted circle). (E) Averaged total volume (μm^3) of the objects per oocyte/embryo. (F, G) Total volumes of the objects sorted by size, or the percentage of each fraction relative to the total volume. (H, I) Numbers of large objects in GV or MII oocytes at a distance of >30 μm (cellular peripheral) or <25 μm (medial) from the cellular center. Significance was examined using one-way ANOVA, and the significance to MII are indicated with asterisks ($P<0.05$). Error bars indicate SEM. Dot plots show mean ± SEM.

Fig. 3. Endosomal-lysosomal organelles form assembly structures, ELYSA.

(A) The internal structure of the giant structure in MII oocytes was analyzed by correlative light and electron microscopy (CLEM) analysis using anti-RAB7 and anti-LAMP1 antibodies. A merged image of immunostaining and electron microscopy (EM) is indicated (left), and a toluidine blue staining image of the adjacent thin section (right) is indicated. Black arrowheads indicate the giant structures positive for RAB7/LAMP1/toluidine blue staining. Note that RAB7/LAMP1 staining is indicated in a pseudo-color. (B) The fluorescent distribution of RAB7/LAMP1 immunostaining was analyzed with deconvolution confocal microscopy. Note that RAB7/LAMP1 staining is indicated in pseudo-color. (C) A series of images of toluidine blue-stained serial semi-thin sections of the Epon-embedded MII oocyte were reconstructed in 3D using oocytes fixed with 2.5% glutaraldehyde (GA). Based on the images obtained, chromosomes were segmented blue, toluidine blue-positive structures were segmented yellow, and the oocyte PM was

segmented white. (D) The internal structures of the toluidine blue-positive structure, ELYSA, were observed using conventional EM of oocytes fixed with 2.5% GA. Magnified regions in a or b (right) are indicated by boxes (left). Arrows, arrowheads, or asterisks indicate vesicles harboring high electron density contents and multilamellar or multivesicular structures, respectively. ELYSA, endosomal lysosomal organellar assembly.

Fig. 4. An autophagy marker LC3 is also detected in ELYSA.

Germinal vesicle (GV) (A) and MII (B) oocytes were fixed and co-stained with anti-LC3 and anti-LAMP1 antibodies. Maximum intensity projection of confocal images at an axial scan range of 80 μm is shown as Z-projection images. Magnified regions (right) are indicated by yellow boxes. DNA was stained with Hoechst 33342. Arrowheads indicate the positions of oocyte chromosomes.

Fig. 5. Enlargement of ELYSA and its redistribution to the cell periphery occur in an actin cytoskeleton-dependent manner.

GV oocytes were incubated for *in vitro* maturation (IVM) for 18 h with or without actin polymerization inhibitors (10 μM latrunculin A or cytochalasin B) or a tubulin inhibitor (20 μM nocodazole), then fixed and co-stained with anti-LC3 and anti-LAMP1 antibodies. The reconstituted objects for LAMP1-positive organelles in 10 oocytes for each treatment from more than three independent experiments were analyzed for the number, size, and distribution. (A) Maximum intensity projection of confocal images at an axial scan range of 80 μm is shown as Z-projection images. DNA was stained with Hoechst 33342.

Arrowheads indicate the metaphase plate. (B) Average total object number per oocyte. (C) Numbers of the objects sorted by size. (D, E) Total volumes of the objects sorted by size, or the percentage of each fraction relative to the total volume. (F, G) Numbers of objects with diameters >4 μm in oocytes at a distance of >30 μm or <25 μm from the cellular center. Significance was examined using one-way ANOVA, and the significance to DMSO are indicated with asterisks ($P<0.05$). Error bars indicate SEM. Dot plots are indicated with mean ± SEM.

Fig. 6. Assembly of ELYSA during migration and limited interaction with the acidification machinery

(A) Snapshots of a time-lapse observation for EGFP fluorescence of GV oocytes injected with *Lamp1-EGFP* and *V1A-mCherry* mRNA are indicated. Maximum intensity projection of confocal images with a height of 40 μm (bottom half of the oocyte) are shown. Magnified perinuclear regions (right) are indicated by yellow boxes. Arrowheads indicate assemblies that adhere to each other in the subsequent frame. (B) Maximum intensity projection of deconvolved confocal images at an axial scan range of 80 μm is shown as Z-projection images. Magnified regions are indicated by yellow boxes (a, b) and the LAMP1-EGFP organelle regions are indicated by yellow dotted line.

Fig. 7. Endosomes and lysosomes in the ELYSA are weakly acidified, but further acidification occurs after the 4-cell stage.

Oocytes and embryos at different stages were stained in the same drop for LysoSensor

Green and LysoTracker Red staining analysis, and confocal images were acquired. Averaged intensity projection of confocal images at an axial scan range of 80 μm is shown as Z-projection images. Magnified ratiometric image for LysoTracker/LysoSensor fluorescence of cytosolic regions indicated by yellow boxes are presented as “fire” look up table images at the bottom. Arrowheads indicate ELYSAs recognized with LysoSensor.

Fig. 8. ATP6V1A localization on acidic vesicles increases as ELYSAs are disassembled.

Embryos injected with *V1A-mCherry* mRNA (at 3 hpf) were incubated to the blastocyst stage in the presence of LysoSensor Green. Snapshots of a time-lapse observation of a representative embryo are shown as maximum intensity projection of confocal images with a height of 80 μm, unless otherwise specified. Magnified perinuclear regions are indicated by yellow boxes.

Fig. 9. Proteolytic activity of cathepsin B is maintained at a relatively low level in the ELYSA.

(A) GV and MII oocytes were stained in the same drop for LysoSensor Green and Magic Red cathepsin B staining analysis, and confocal images were acquired. (B) Fluorescent intensities of LysoSensor and Magic Red on the yellow lines indicated in (A) are indicated by a line plot. Small, filled dots indicate the origin (0 μm) in distance.

Supplementary Fig. 1. Endosomes and lysosomes form giant structures in the periphery of the oocyte plasma membrane.

MII oocytes were fixed and co-stained with anti-RAB7 and anti-LAMP1 antibodies. The schematic diagram indicates the location of oocyte chromosomes and the metaphase plate in the MII oocytes. Maximum intensity projection of confocal images at an axial scan range of 80 μm is shown as Z-projection images. Arrowheads indicate the positions of oocyte chromosomes.

Supplementary Fig. 2. Schemes of the three-dimensional particle analysis in this study. Oocytes/embryos were fixed and stained, and three-dimensional images were acquired as serial z-stack images using confocal microscopy. Fields to analyze were cropped for each oocyte/embryo, and the upper and lower end of LAMP1 fluorescent signals in cytosol were examined and used to determine the center plane of the cell. The cellular region in the center plane was used for masking and determination of the geometric center (as a 3D center of the oocyte). Deletion of the signals from the polar body or zona pellucida was carried out manually. Signals on PM were eliminated by both size exclusion of 3D particle counter plugin in Fiji software and by manual erasing. The distal distance of each particle from the 3D center of the oocyte was used for the distribution study to avoid underestimation of the distance of large ELYSA particle, which was calculated by adding the 3D distance from the center of cell to the geometric center of the particle and the mean diameter of the particle.

Supplementary Fig. 3. Giant structures in MII oocytes were immunostained with anti-RAB7 and LAMP1 antibodies after glutaraldehyde (GA) fixation.

MII oocytes were fixed with 0.025% GA and co-stained with anti-RAB5/RAB7 and anti-LAMP1 antibodies. Single-section images from confocal observation are shown.

Supplementary Fig. 4. Toluidine blue-positive structures in MII oocytes show similar localization patterns to the ELYSA.

Aligned serial toluidine blue-stained light microscopic images were stacked and three-dimensionally reconstructed by inversing the intensity and adjusting it to be transparent.

Supplementary Fig. 5. An early endosome marker RAB5 is localized within the ELYSA in the presence of inhibitors for cytoskeletons.

GV oocytes were incubated for *in vitro* maturation (IVM) for 18 h with or without inhibitors of polymerized actin (10 μM latrunculin A or cytochalasin B) or tubulin (20 μM nocodazole), and fixed and co-stained with anti-RAB5 and anti-LAMP1 antibodies. Maximum intensity projection of confocal images at an axial scan range of 80 μm is shown as Z-projection images. Magnified regions are indicated by yellow boxes. DNA was stained with Hoechst 33342. Arrowhead indicates the metaphase plate.

Supplementary Fig. 6. LysoTracker-positive punctate structures colocalized with V1A-mCherry.

Embryos were injected with V1A-mCherry mRNA (at 3 hpf) and cultured with or without bafilomycin A_1 and stained with LysoTracker Green at the indicated time points. Maximum

intensity projection of confocal images at an axial scan range of 80 μm is shown as Z-projection images.

Supplementary Fig. 7. Magic Red cathepsin B staining showed positive signals in the cytoplasm as well as the ELYSA in GV and MII oocytes.

Oocytes and embryos at the indicated stages were collected and stained with Magic Red Cathepsin B solution in the same drop of medium. Averaged intensity projection of confocal images at an axial scan range of 80 μm is shown as Z-projection images.

Video 1.

MII oocytes were fixed and co-stained with anti-RAB5 and anti-LAMP1 antibodies. A series of the confocal images with a height of 80 μm is shown from top to bottom.

Video 2.

A series of continuous toluidine blue-stained light microscopic images of the same oocyte (top half) reconstructed to 3D. Chromosomes in the images obtained were segmented blue, toluidine blue-positive structures were segmented yellow, and oocyte PM was segmented white.

Video 3.

GV oocytes were injected with the mixture mRNA solution for *Lamp1-EGFP* and *V1A-mCherry*, and incubated for IVM. Time-lapse movie of EGFP fluorescence of a

representative oocyte is indicated as maximum intensity projection of confocal images with a height of 80 μm. Magnified perinuclear regions in Fig. 5 are indicated by a box. The timestamp indicates the time after IVM started.

Video 4

GV oocytes were injected with V1A-mCherry mRNA and incubated for 18 h for IVM in the presence of LysoSensor green. Fluorescent images of a representative oocyte which matured to MII stage is presented. A series of the confocal images of 81 slices with a height of 80 μm is shown from top to bottom.

Video 5.

Embryos were injected with V1A-mCherry mRNA at 3 hpf and incubated for further embryogenesis in the presence of LysoSensor Green during embryonic development. A time-lapse movie of a representative embryo is shown (maximum intensity projection of confocal images at a height of 80 μm).

Figure 1

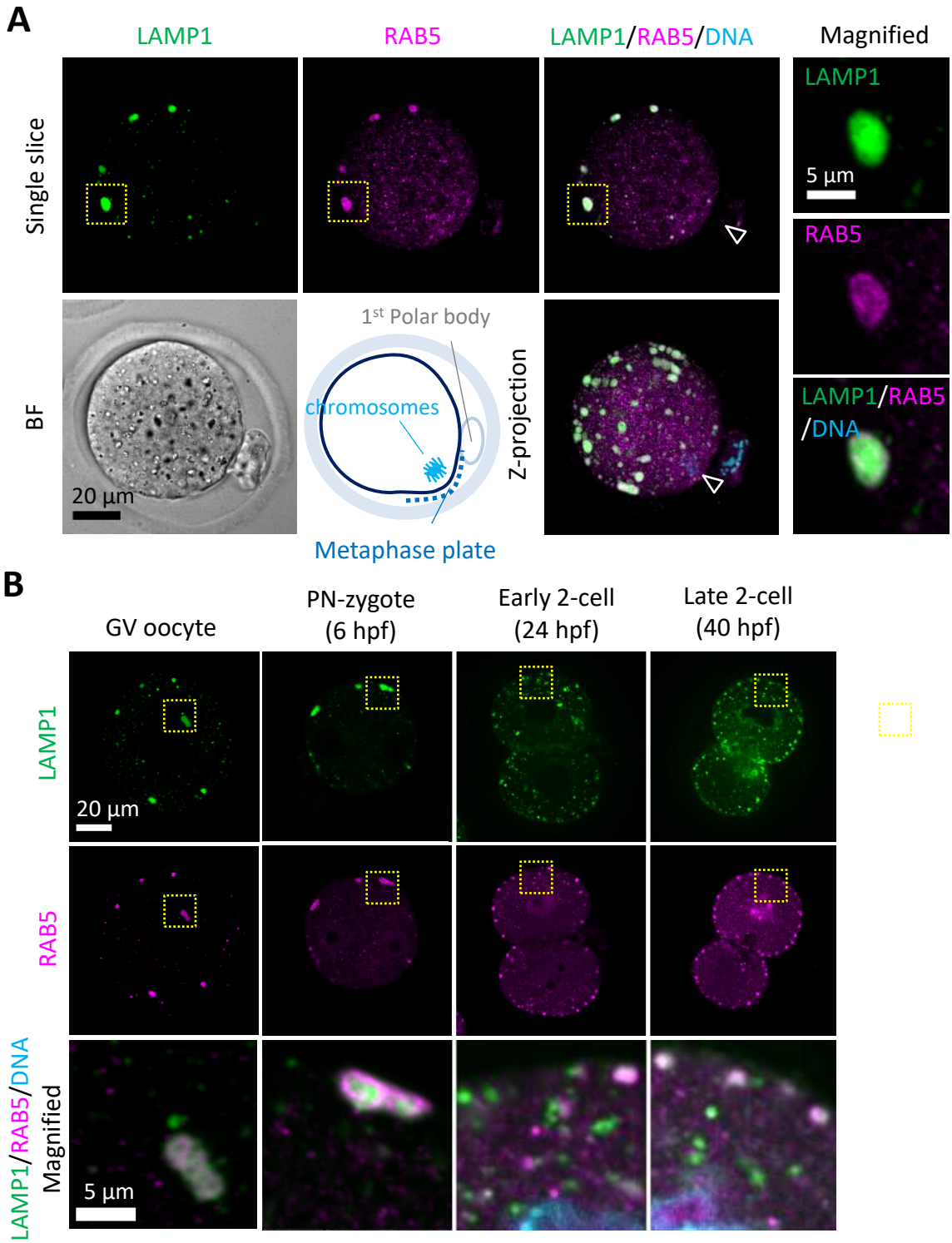

Fig. 1. Endosomes and lysosomes form giant structures in the periphery of the oocyte plasma membrane. (A) Meiosis II (MII) oocytes were fixed and co-stained with anti-RAB5 and anti-LAMP1 antibodies. The schematic diagram indicates the location of oocyte chromosomes and metaphase plate in the MII oocytes. Maximum intensity projection of confocal images at an axial scan range of 80 µm is shown as Z-projection images. Arrowheads indicate the positions of oocyte chromosomes. Magnified regions (right) are indicated by yellow boxes. (B) Embryos at different stages were fixed and co-stained with anti-RAB5 and anti-LAMP1 antibodies. Hour(s) post-fertilization is indicated as hpf. DNA was stained with Hoechst 33342.

Figure 2

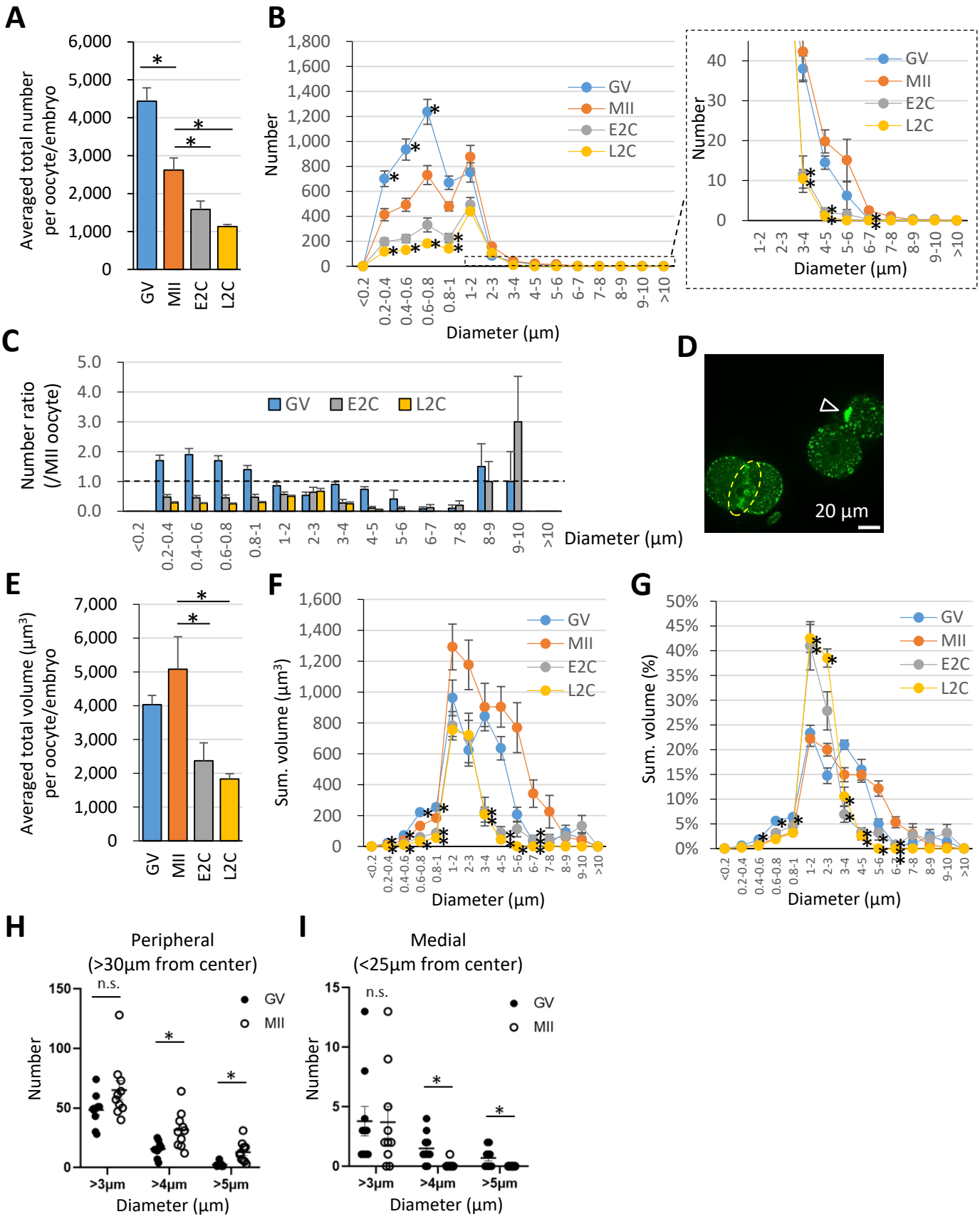
A
Averaged total number per oocyte/embryo
6,000
5,000
4,000
3,000
2,000
1,000
0
GV
MII
E2C
L2C
B
Number
1,800
1,600
1,400
1,200
1,000
800
600
400
200
0
GV
MII
E2C
L2C
<0.2
0.2-0.4
0.4-0.6
0.6-0.8
0.8-1
1-2
2-3
3-4
4-5
5-6
6-7
7-8
8-9
9-10
>10
Diameter (μm)
40
30
20
10
0
C
Number ratio (/MII oocyte)
5.0
4.0
3.0
2.0
1.0
0.0
GV
E2C
L2C
Diameter (μm)
D
20 μm
E
Averaged total volume (μm³) per oocyte/embryo
7,000
6,000
5,000
4,000
3,000
2,000
1,000
0
F
Sum. volume (μm³)
1,600
1,400
1,200
1,000
800
600
400
200
0
G
Sum. volume (%)
50%
45%
40%
35%
30%
25%
20%
15%
10%
5%
0%
H
Peripheral
(>30μm from center)
n.s.
Number
150
100
50
0
GV
MII
>3μm
>4μm
>5μm
Diameter (μm)
I
Medial
(<25μm from center)
n.s.
Number
15
10
5
0
GV
MII
>3μm
>4μm
>5μm
Diameter (μm)

Fig. 2. Endosomes and lysosomes form giant structures in the periphery of the MII oocyte PM
Germinal vesicle (GV) oocyte, MII oocyte, early 2-cell (E2C: 24 hpf), and late 2-cell (L2C: 40 hpf) embryos were fixed and stained with anti-LAMP1 antibody. Reconstituted three-dimensional objects for the LAMP1-positive organelles in 9 to 10 oocytes for each stage from more than three independent experiments were further analyzed for number, size and distribution. (A) Averaged total object number per oocyte/embryo. (B) Numbers of the objects sorted by size (indicated by the diameters of spheres calculated from volumes) with an inset indicating an enlarged graph of the dotted region. (C) Ratios of (B) to the average of MII oocyte, (D) A single confocal section image for E2C embryos which have transient and concatenated objects upon cellular division (arrowhead) and a prominent signal on the PM of cleavage furrow (dotted circle). (E) Averaged total volume (μm^3) of the objects per oocyte/embryo. (F, G) Total volumes of the objects sorted by size, or the percentage of each fraction relative to the total volume. (H, I) Numbers of large objects in GV or MII oocytes at a distance of >30 μm (cellular peripheral) or <25 μm (medial) from the cellular center. Significance was examined using one-way ANOVA, and the significance to MII are indicated with asterisks ($P<0.05$). Error bars indicate SEM. Dot plots show mean ± SEM.

Figure 3

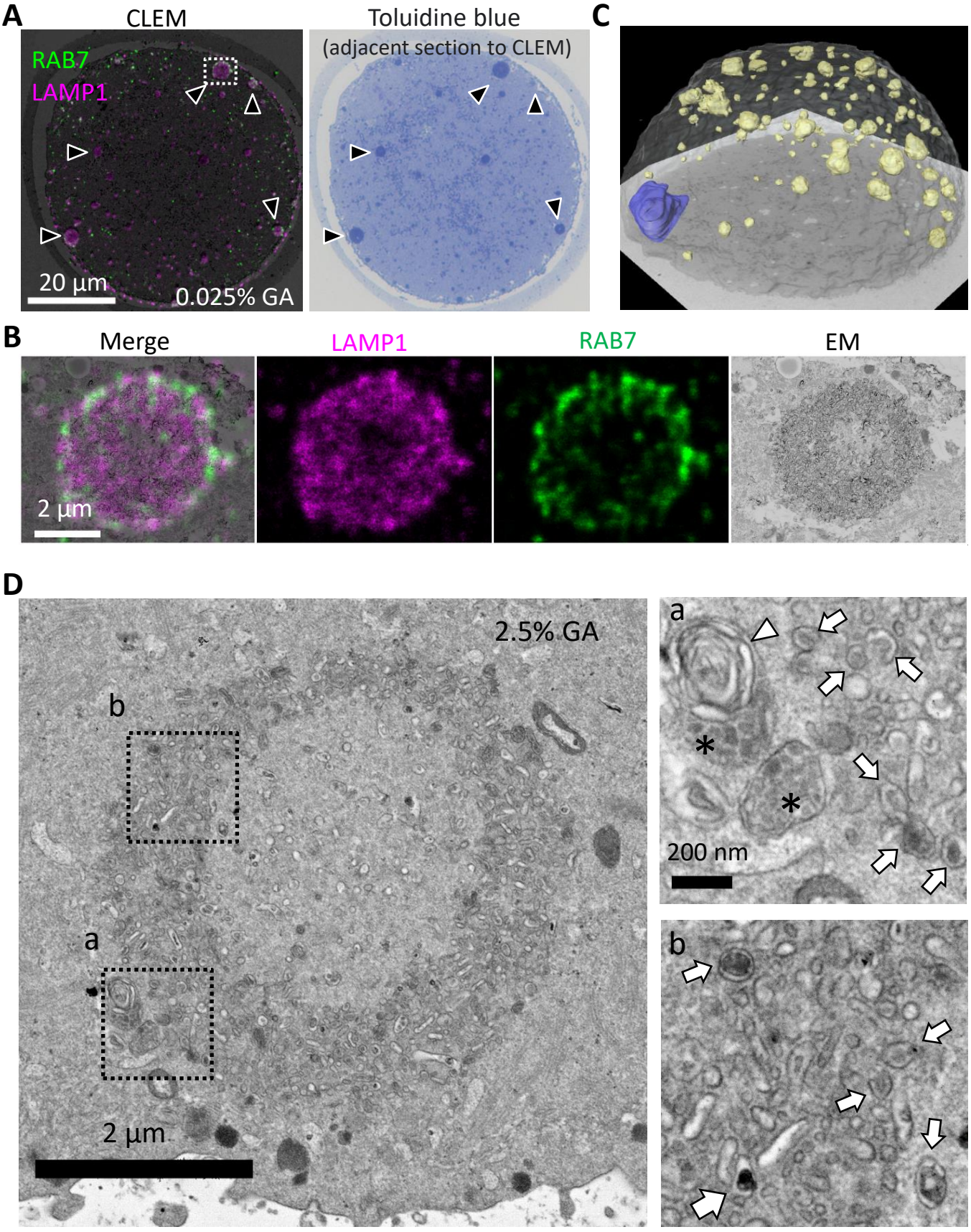
A
CLEM
RAB7
LAMP1
20 µm
0.025% GA
Toluidine blue
(adjacent section to CLEM)
C
B
Merge
LAMP1
RAB7
EM
2 µm
D
2.5% GA
b
a
2 µm
a
200 nm
b

Fig. 3. Endosomal-lysosomal organelles form assembly structures, ELYSA.
(A) The internal structure of the giant structure in MII oocytes was analyzed by correlative light and electron microscopy (CLEM) analysis using anti-RAB7 and anti-LAMP1 antibodies. A merged image of immunostaining and electron microscopy (EM) is indicated (left), and a toluidine blue staining image of the adjacent thin section (right) is indicated. Black arrowheads indicate the giant structures positive for RAB7/LAMP1/toluidine blue staining. Note that RAB7/LAMP1 staining is indicated in a pseudo-color. (B) The fluorescent distribution of RAB7/LAMP1 immunostaining was analyzed with deconvolution confocal microscopy. Note that RAB7/LAMP1 staining is indicated in pseudo-color.(C) A series of images of toluidine blue-stained serial semi-thin sections of the Epon-embedded MII oocyte were reconstructed in 3D. Based on the images obtained, chromosomes were segmented blue, toluidine blue-positive structures were segmented yellow, and the oocyte PM was segmented white. (D) The internal structures of the toluidine blue-positive structure, ELYSA, were observed using conventional EM of oocytes fixed with 2.5% glutaraldehyde (GA). Magnified regions in a or b (right) are indicated by boxes (left). Arrows, arrowheads, or asterisks indicate vesicles harboring high electron density contents and multilamellar or multivesicular structures, respectively. ELYSA, endosomal lysosomal organellar assembly.

Figure 4

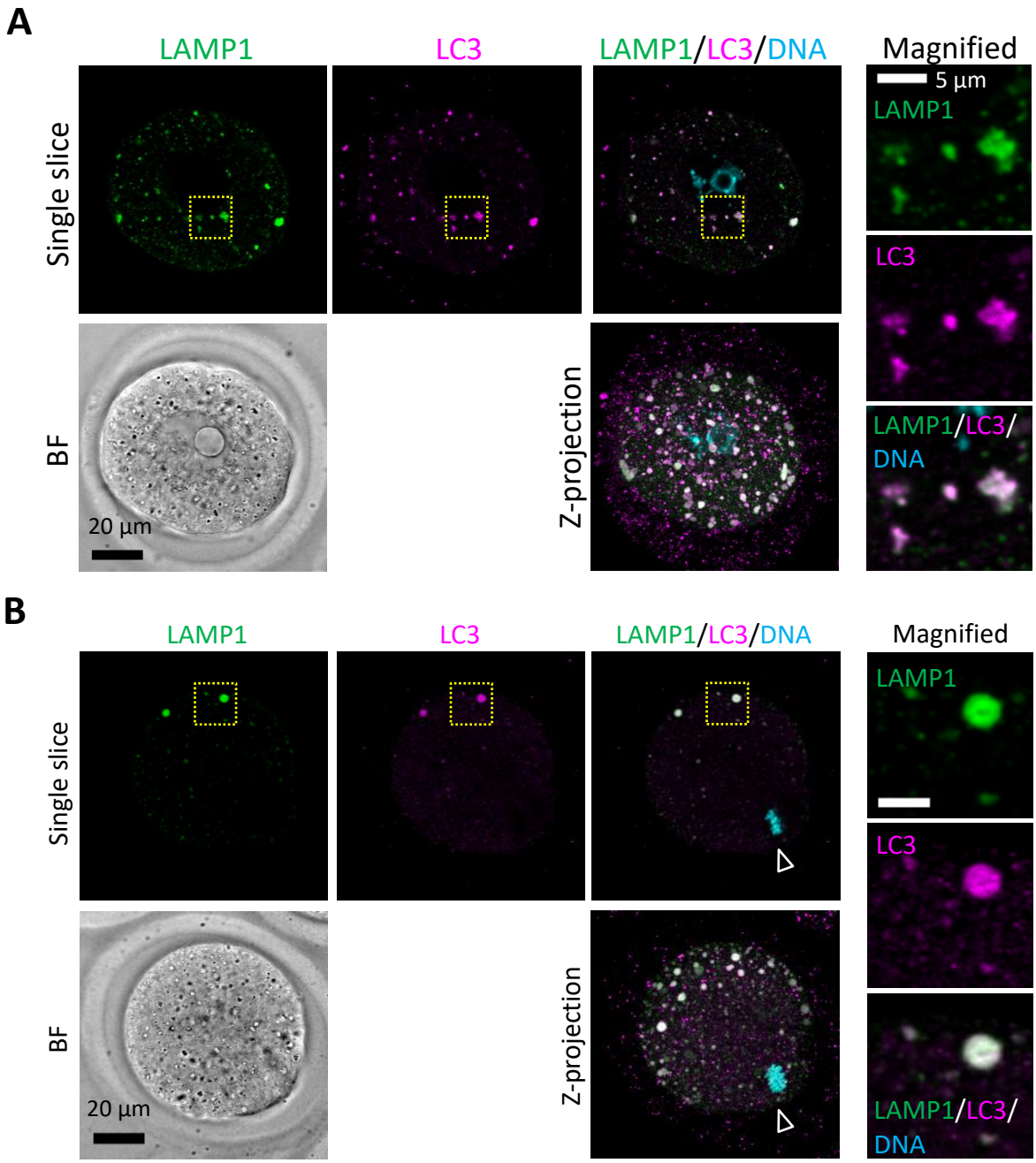

Fig. 4. An autophagy marker LC3 is also detected in ELYSA.
Germinal vesicle (GV) (A) and MII (B) oocytes were fixed and co-stained with anti-LC3 and anti-LAMP1 antibodies. Maximum intensity projection of confocal images at an axial scan range of 80 µm is shown as Z-projection images. Magnified regions (right) are indicated by yellow boxes. DNA was stained with Hoechst 33342. Arrowheads indicate the positions of oocyte chromosomes.

Figure 5

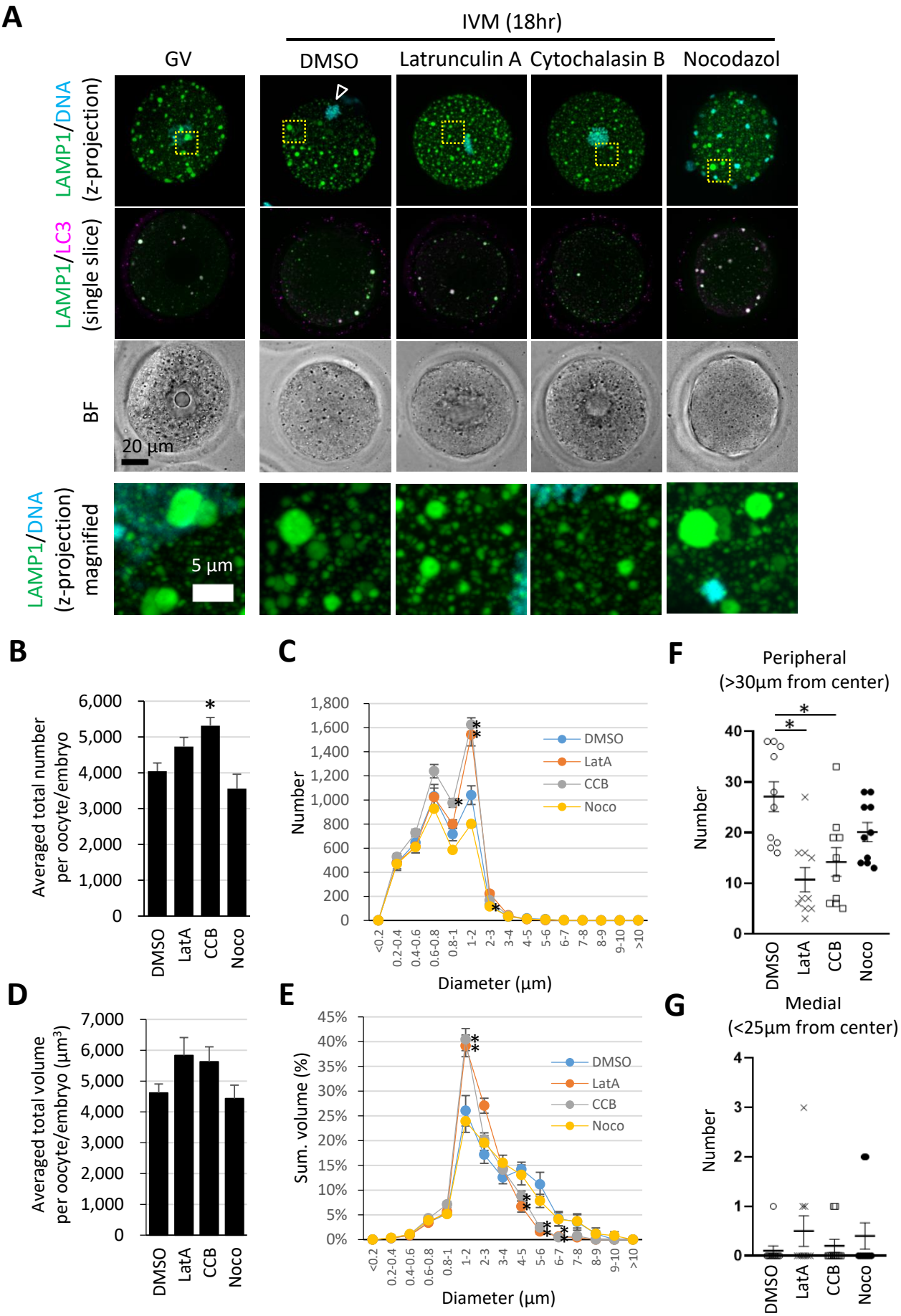
A
IVM (18hr)
GV
DMSO
Latrunculin A
Cytochalasin B
Nocodazol
LAMP1/DNA (z-projection)
LAMP1/LC3 (single slice)
BF
20 µm
LAMP1/DNA (z-projection) magnified
5 µm
B
Averaged total number per oocyte/embryo
DMSO
LatA
CCB
Noco
C
Number
Diameter (µm)
D
Averaged total volume per oocyte/embryo (µm³)
E
Sum. volume (%)
F
Peripheral (>30µm from center)
G
Medial (<25µm from center)

Fig. 5. Enlargement of ELYSA and its redistribution to the cell periphery occur in an actin cytoskeleton-dependent manner.

GV oocytes were incubated for *in vitro* maturation (IVM) for 18 h with or without actin polymerization inhibitors (10 μM latrunculin A or cytochalasin B) or a tubulin inhibitor (20 μM nocodazole), then fixed and co-stained with anti-LC3 and anti-LAMP1 antibodies. The reconstituted objects for LAMP1-positive organelles in 10 oocytes for each treatment from more than three independent experiments were analyzed for the number, size, and distribution. (A) Maximum intensity projection of confocal images at an axial scan range of 80 μm is shown as Z-projection images. DNA was stained with Hoechst 33342. Arrowheads indicate the metaphase plate. (B) Average total object number per oocyte. (C) Numbers of the objects sorted by size. (D, E) Total volumes of the objects sorted by size, or the percentage of each fraction relative to the total volume. (F, G) Numbers of objects with diameters >4 μm in oocytes at a distance of >30 μm or <25 μm from the cellular center. Significance was examined using one-way ANOVA, and the significance to DMSO are indicated with asterisks ($P<0.05$). Error bars indicate SEM. Dot plots are indicated with mean ± SEM.

Figure 6

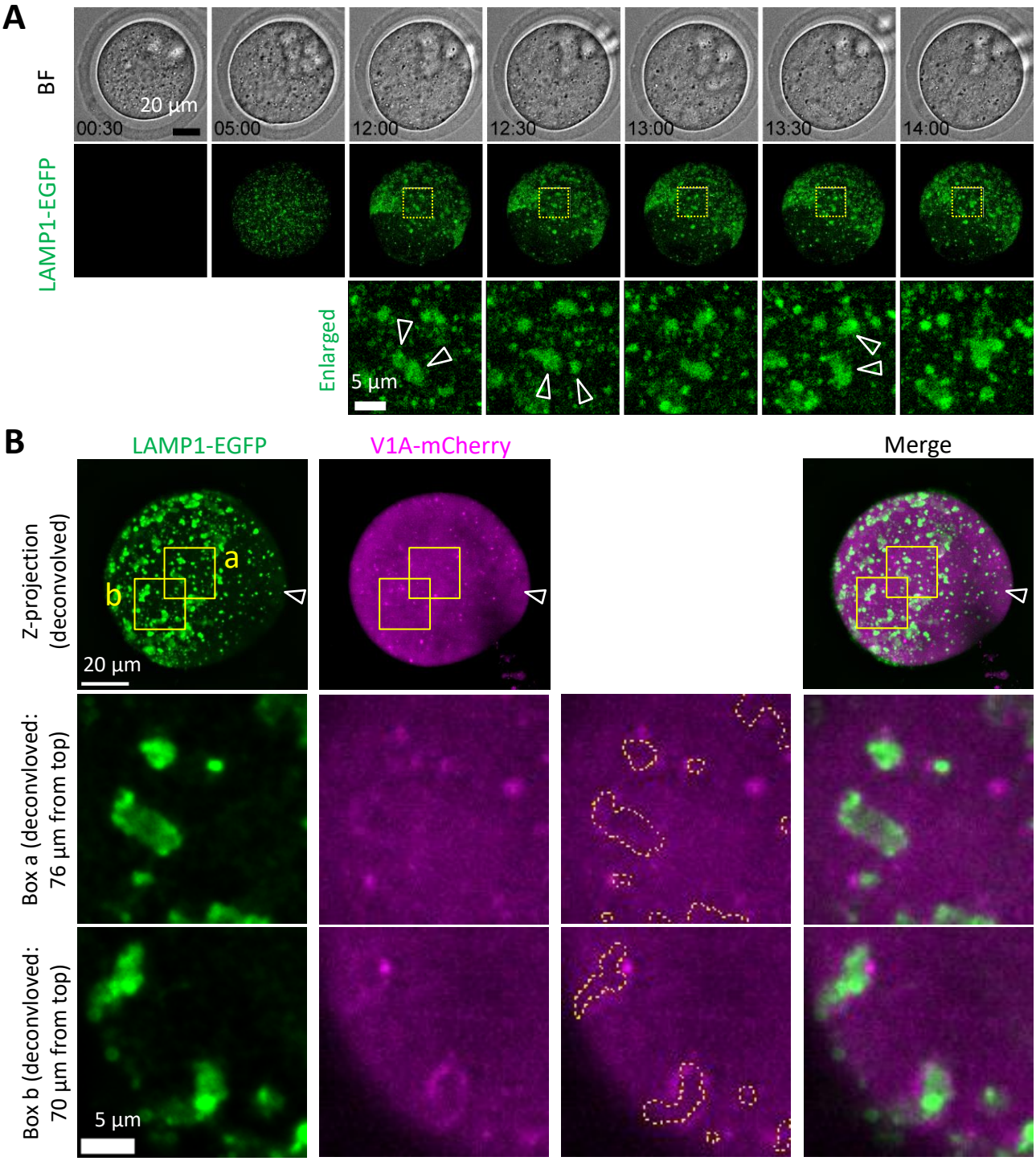

Fig. 6. Assembly of ELYSA during migration and limited interaction with the acidification machinery
(A) Snapshots of a time-lapse observation for EGFP fluorescence of GV oocytes injected with *Lamp1-EGFP* and *V1A-mCherry* mRNA are indicated. Maximum intensity projection of confocal images with a height of 40 µm (bottom half of the oocyte) are shown. Magnified perinuclear regions (right) are indicated by yellow boxes. Arrowheads indicate assemblies that adhere to each other in the subsequent frame. (B) Maximum intensity projection of deconvolved confocal images at an axial scan range of 80 µm is shown as Z-projection images. Magnified regions are indicated by yellow boxes (a, b) and the LAMP1-EGFP organelle regions are indicated by yellow dotted line.

Figure 7

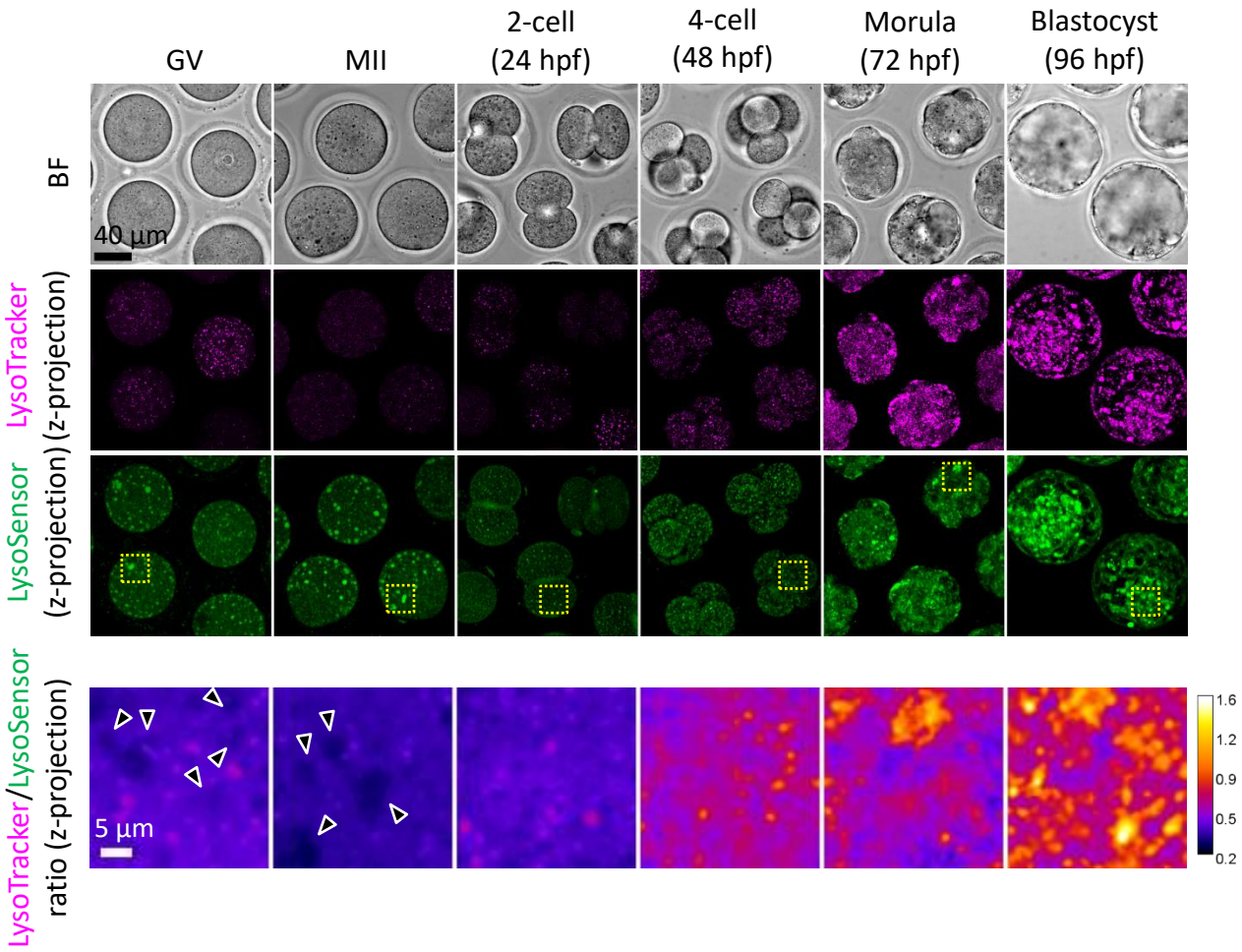

Fig. 7. Endosomes and lysosomes in the ELYSA are weakly acidified, but further acidification occurs after the 4-cell stage.

Oocytes and embryos at different stages were stained in the same drop for LysoSensor Green and LysoTracker Red staining analysis, and confocal images were acquired. Averaged intensity projection of confocal images at an axial scan range of 80 µm is shown as Z-projection images. Magnified ratiometric image for LysoTracker/LysoSensor fluorescence of cytosolic regions indicated by yellow boxes are presented as “fire” look up table images at the bottom. Arrowheads indicate ELYSAs recognized with LysoSensor.

Figure 8

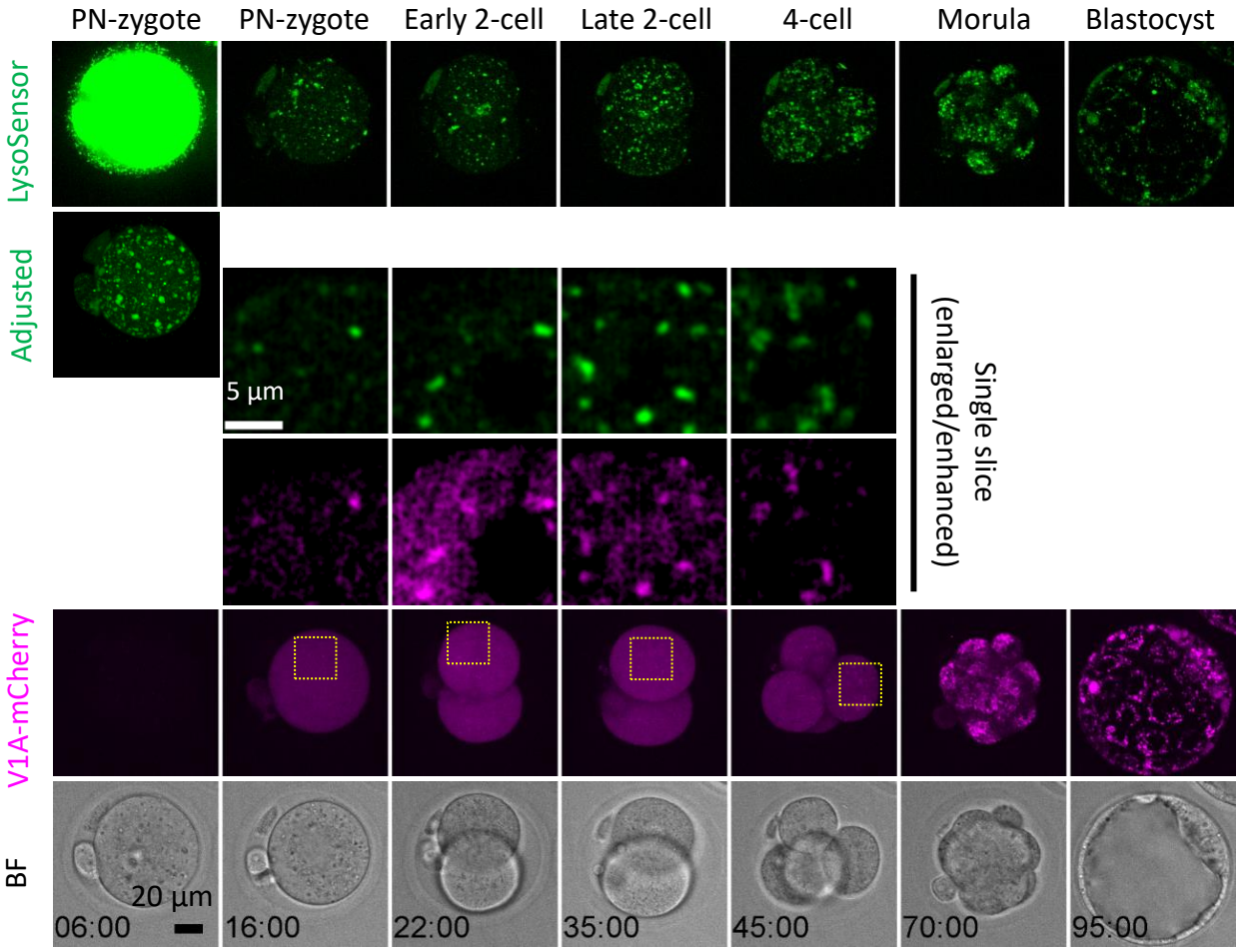

Fig. 8. ATP6V1A localization on acidic vesicles increases as ELYSAs are disassembled. Embryos injected with *V1A-mCherry* mRNA (at 3 hpf) were incubated to the blastocyst stage in the presence of LysoSensor Green. Snapshots of a time-lapse observation of a representative embryo are shown as maximum intensity projection of confocal images with a height of 80 µm, unless otherwise specified. Magnified perinuclear regions are indicated by yellow boxes.

Figure 9

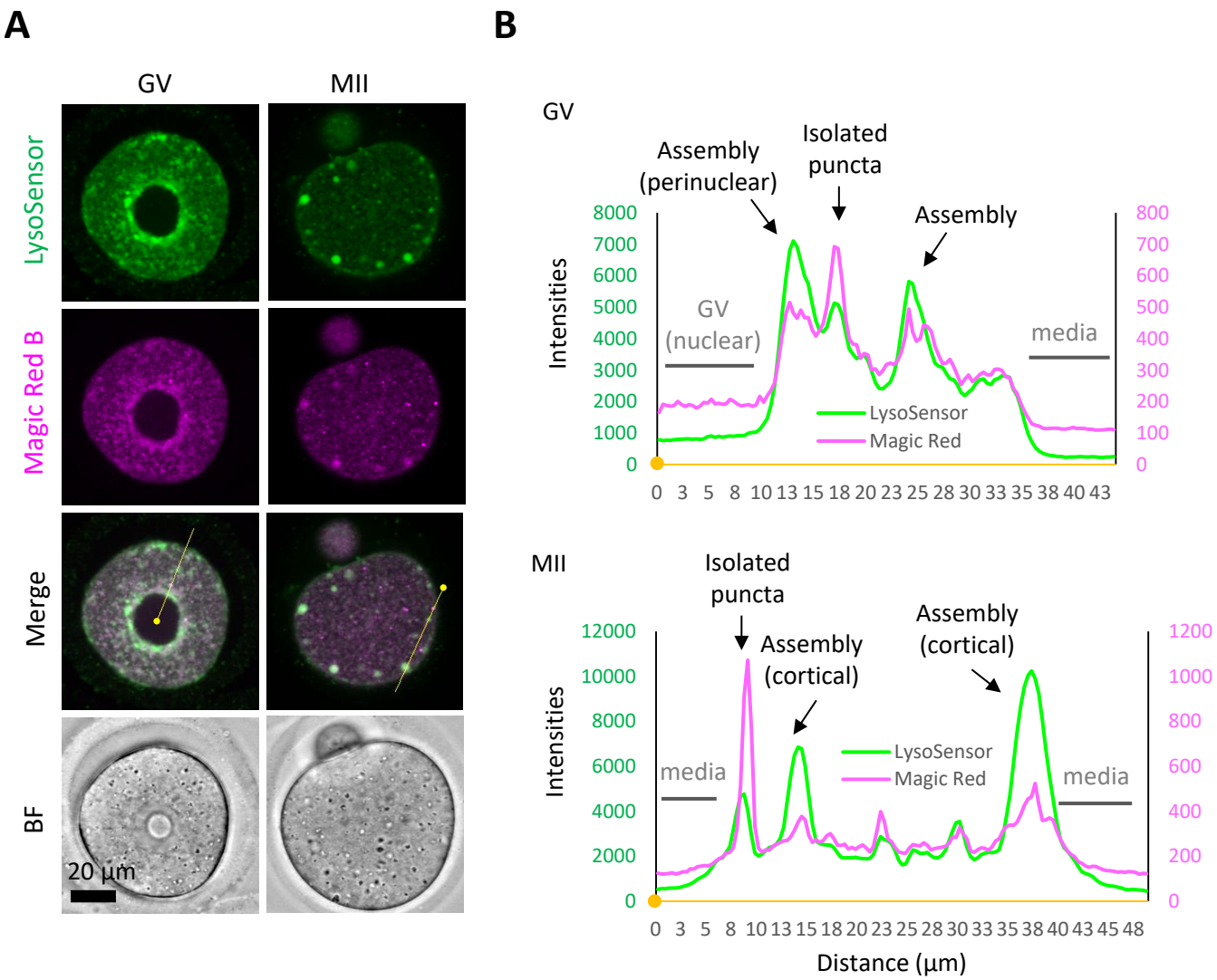

Fig. 9. Proteolytic activity of cathepsin B is maintained at a relatively low level in the ELYSA. (A) GV and MII oocytes were stained in the same drop for LysoSensor Green and Magic Red cathepsin B staining analysis, and confocal images were acquired. (B) Fluorescent intensities of LysoSensor and Magic Red on the yellow lines indicated in (A) are indicated by a line plot. Small, filled dots indicate the origin (0 µm) in distance.

Supplementary Figure 1

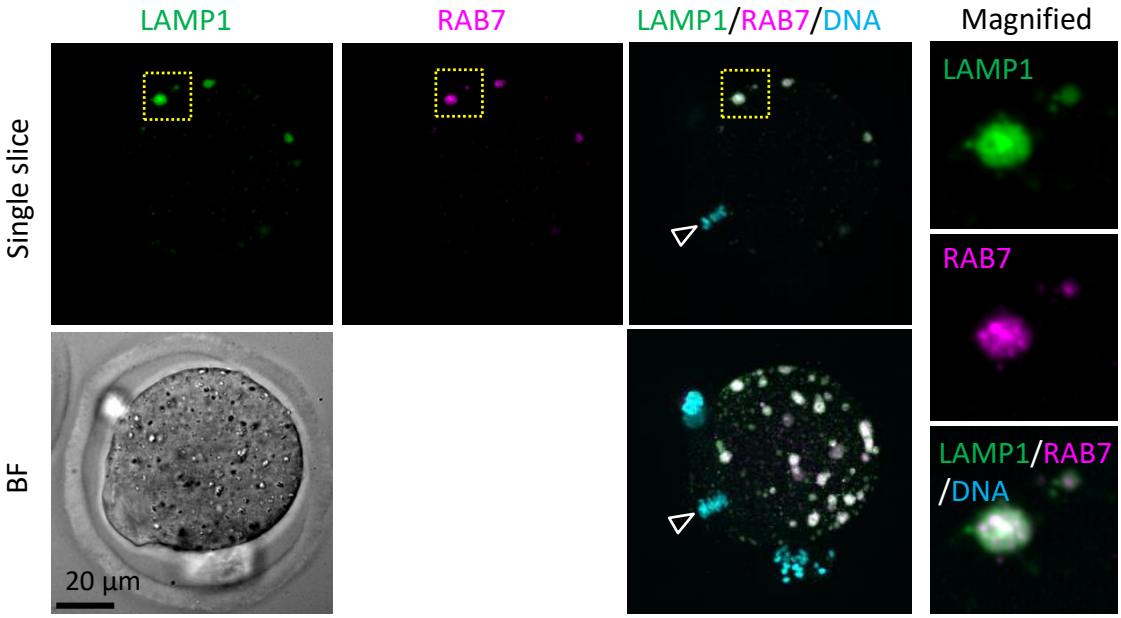

Supplementary Fig. 1. Endosomes and lysosomes form giant structures in the periphery of the oocyte plasma membrane.
MII oocytes were fixed and co-stained with anti-RAB7 and anti-LAMP1 antibodies. The schematic diagram indicates the location of oocyte chromosomes and the metaphase plate in the MII oocytes. Maximum intensity projection of confocal images at an axial scan range of 80 µm is shown as Z-projection images. Arrowheads indicate the positions of oocyte chromosomes.

Supplementary Figure 2

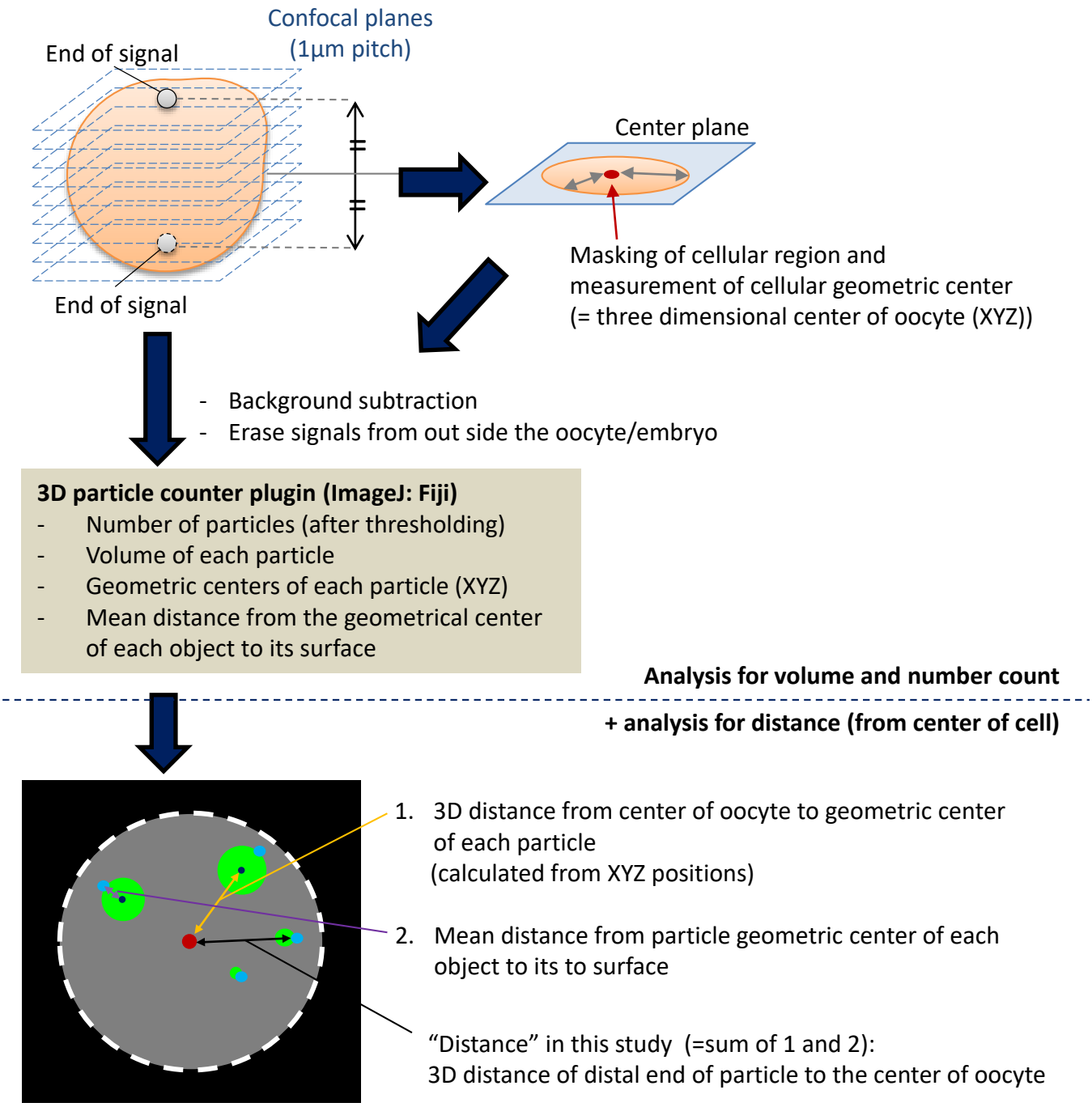

Supplementary Fig. 2. Schemes of the three-dimensional particle analysis in this study.
Oocytes/embryos were fixed and stained, and three-dimensional images were acquired as serial z-stack images using confocal microscopy. Fields to analyze were cropped for each oocyte/embryo, and the upper and lower end of LAMP1 fluorescent signals in cytosol were examined and used to determine the center plane of the cell. The cellular region in the center plane was used for masking and determination of the geometric center (as a 3D center of the oocyte). Deletion of the signals from the polar body or zona pellucida was carried out manually. Signals on PM were eliminated by both size exclusion of 3D particle counter plugin in Fiji software and by manual erasing. The distal distance of each particle from the 3D center of the oocyte was used for the distribution study to avoid underestimation of the distance of large ELYSA particle, which was calculated by adding the 3D distance from the center of cell to the geometric center of the particle and the mean diameter of the particle.

Supplementary Figure 3

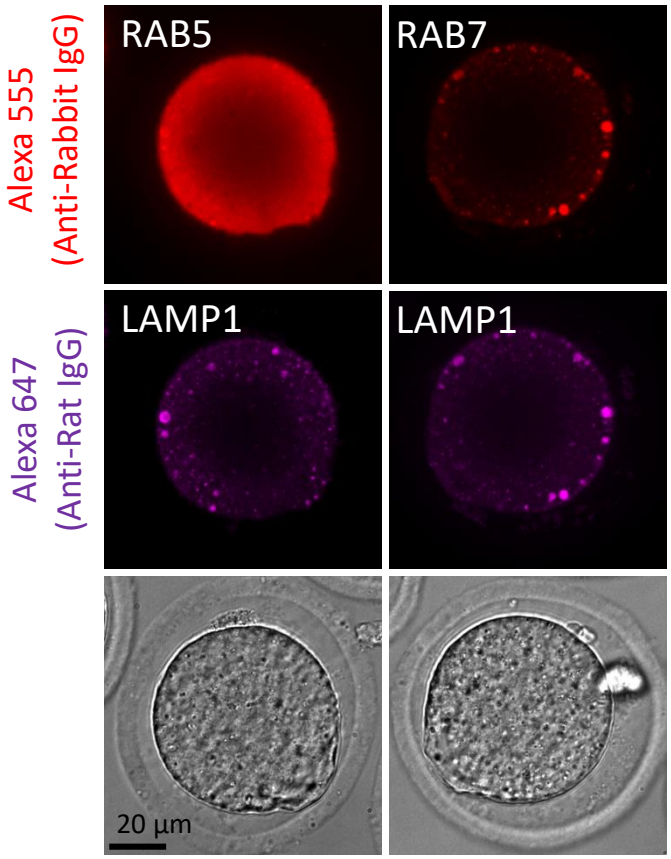

Supplementary Fig. 3. Giant structures in MII oocytes were immunostained with anti-RAB7 and LAMP1 antibodies after glutaraldehyde (GA) fixation.
MII oocytes were fixed with 0.025% GA and co-stained with anti-RAB5/RAB7 and anti-LAMP1 antibodies. Single-section images from confocal observation are shown.

Supplementary Figure 4

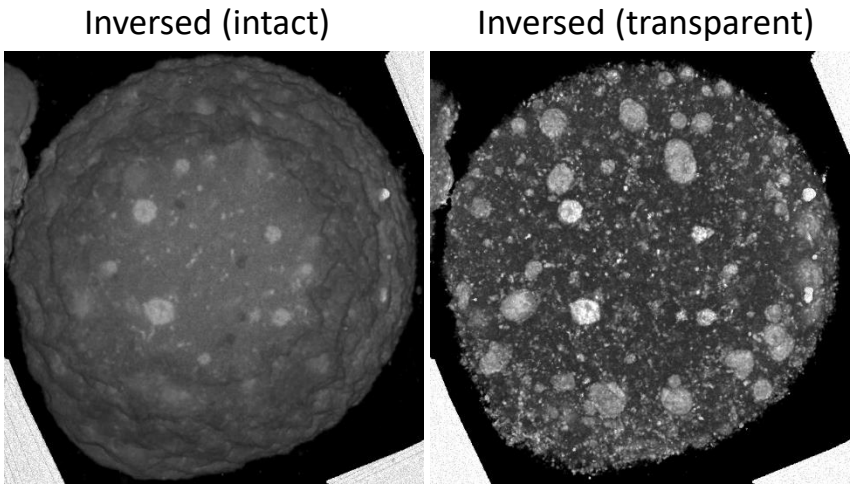

Supplementary Fig. 4. Toluidine blue-positive structures in MII oocytes show similar localization patterns to the ELYSA.
Aligned serial toluidine blue-stained light microscopic images were stacked and three-dimensionally reconstructed by inversing the intensity and adjusting it to be transparent.

Supplementary Figure 5

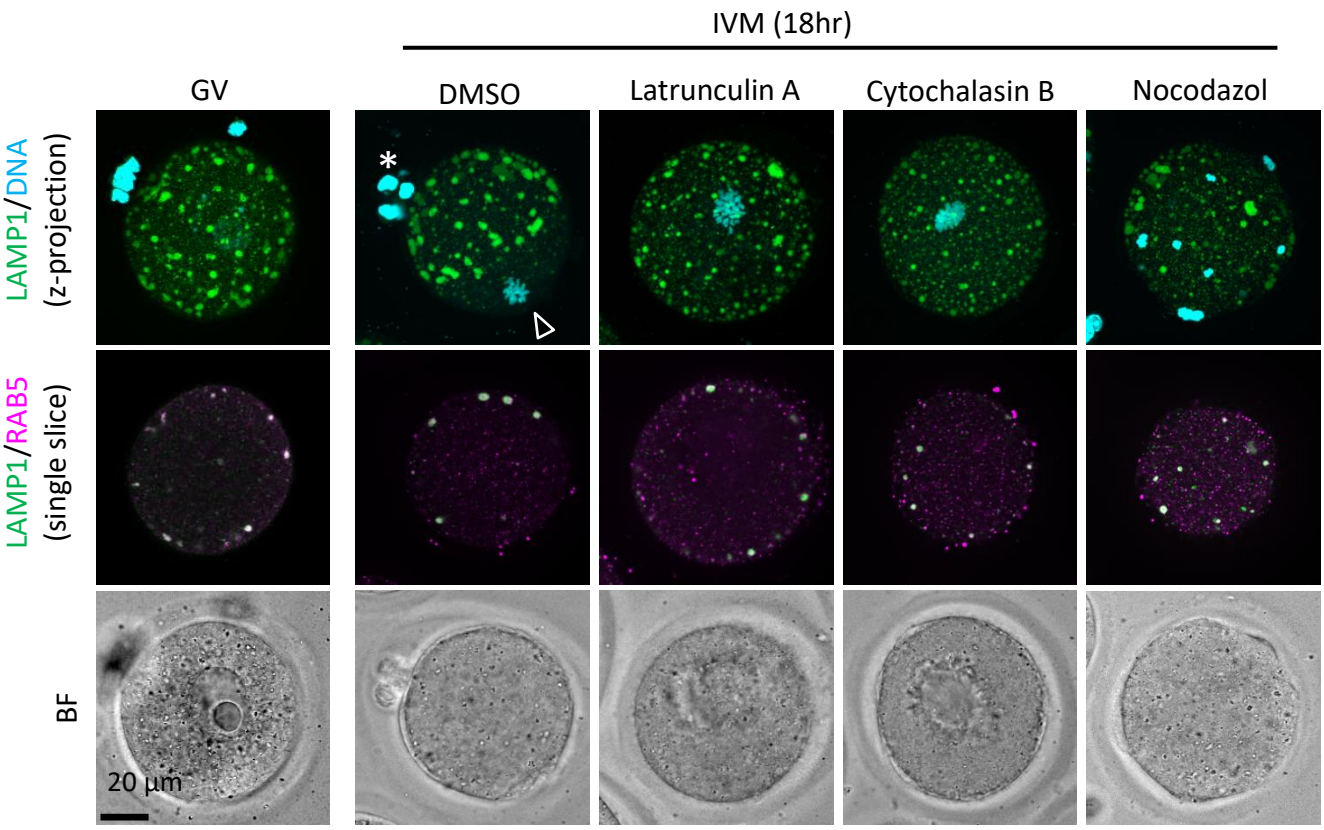

Supplementary Fig. 5. An early endosome marker RAB5 is localized within the ELYSA in the presence of inhibitors for cytoskeletons.
GV oocytes were incubated for *in vitro* maturation (IVM) for 18 h with or without inhibitors of polymerized actin (10 µM latrunculin A or cytochalasin B) or tubulin (20 µM nocodazole), and fixed and co-stained with anti-RAB5 and anti-LAMP1 antibodies. Maximum intensity projection of confocal images at an axial scan range of 80 µm is shown as Z-projection images. Magnified regions are indicated by yellow boxes. DNA was stained with Hoechst 33342. Arrowhead and asterisk indicate the metaphase plate and first polar body, respectively.

Supplementary Figure 6

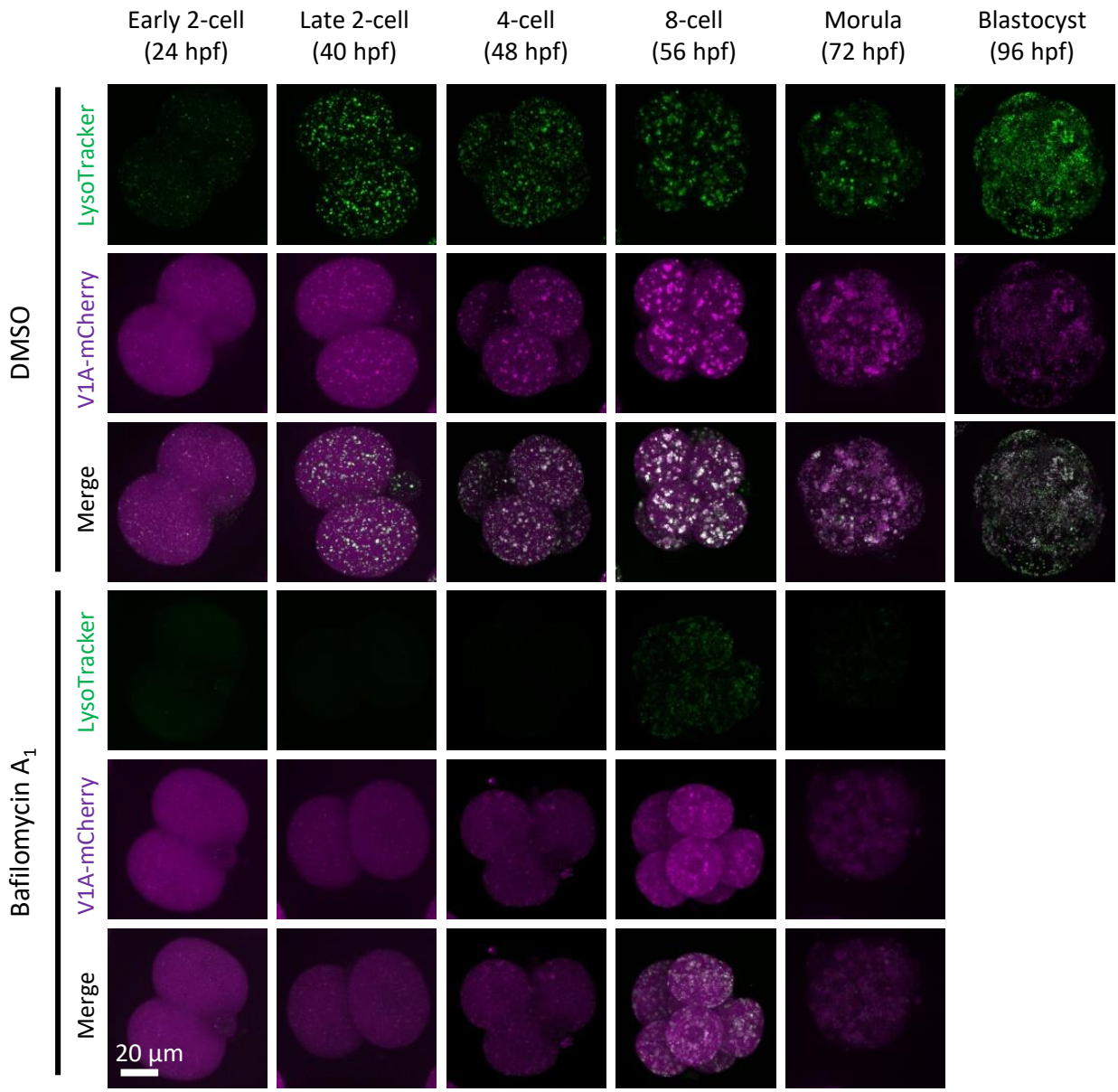

Supplementary Fig. 6. LysoTracker-positive punctate structures colocalized with V1A-mCherry. Embryos were injected with V1A-mCherry mRNA (at 3 hpf) and cultured with or without bafilomycin A_1 and stained with LysoTracker Green at the indicated time points. Maximum intensity projection of confocal images at an axial scan range of 80 µm is shown as Z-projection images.

Supplementary Figure 7

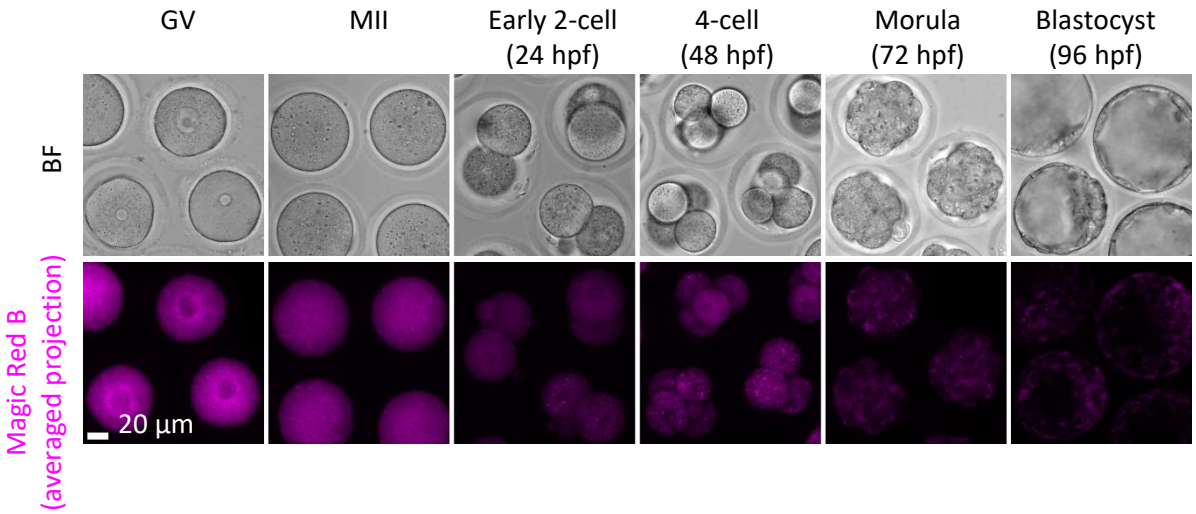

Supplementary Fig. 7. Magic Red cathepsin B staining showed positive signals in the cytoplasm as well as the ELYSA in GV and MII oocytes.
Oocytes and embryos at the indicated stages were collected and stained with Magic Red Cathepsin B solution in the same drop of medium. Averaged intensity projection of confocal images at an axial scan range of 80 µm is shown as Z-projection images.

Video 1

Video 1.
MII oocytes were fixed and co-stained with anti-RAB5 and anti-LAMP1 antibodies. A series of the confocal images with a height of 80 μm is shown from top to bottom.

Video 2

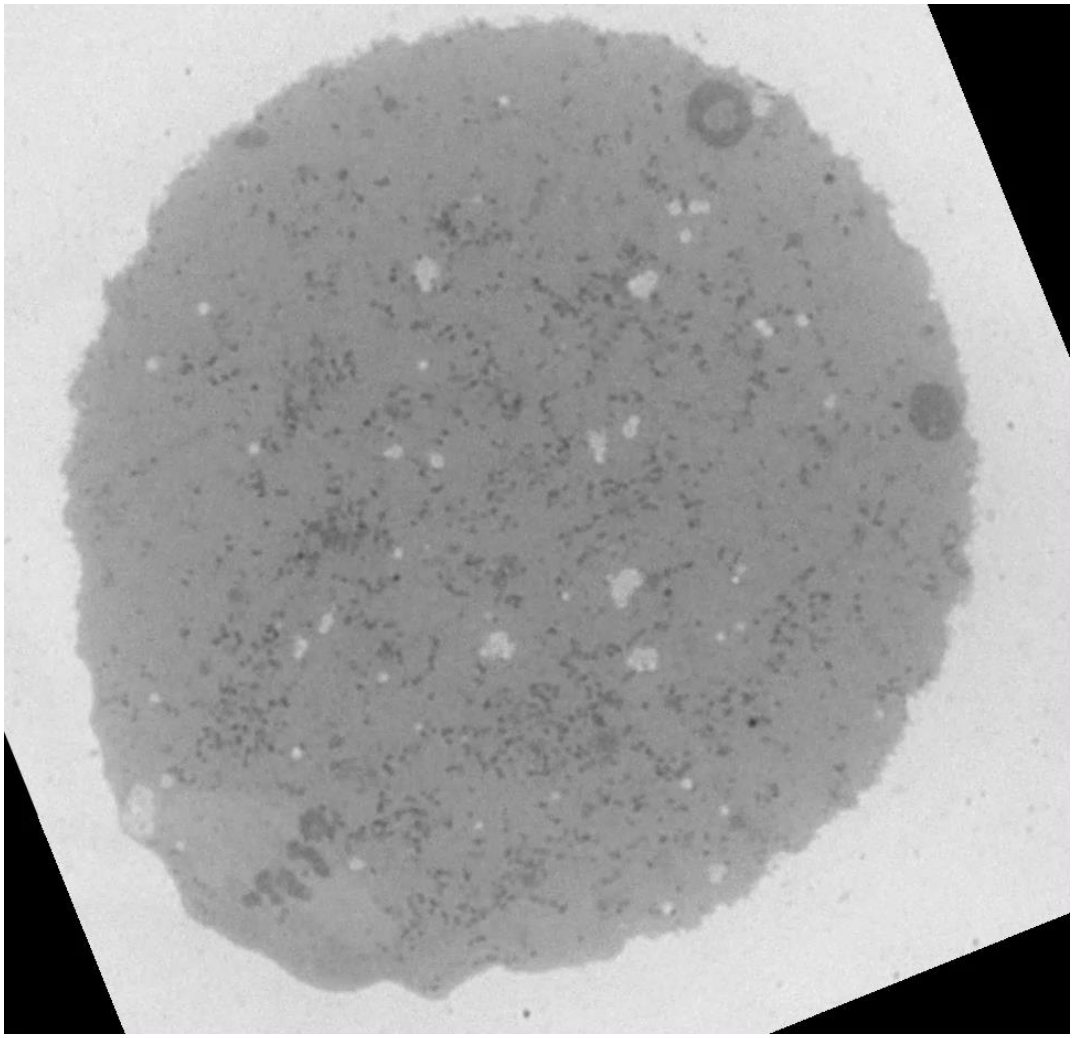

Video 2.
A series of continuous toluidine blue-stained light microscopic images of the same oocyte (top half) reconstructed to 3D. Chromosomes in the images obtained were segmented blue, toluidine blue-positive structures were segmented yellow, and oocyte PM was segmented white.

Video 3

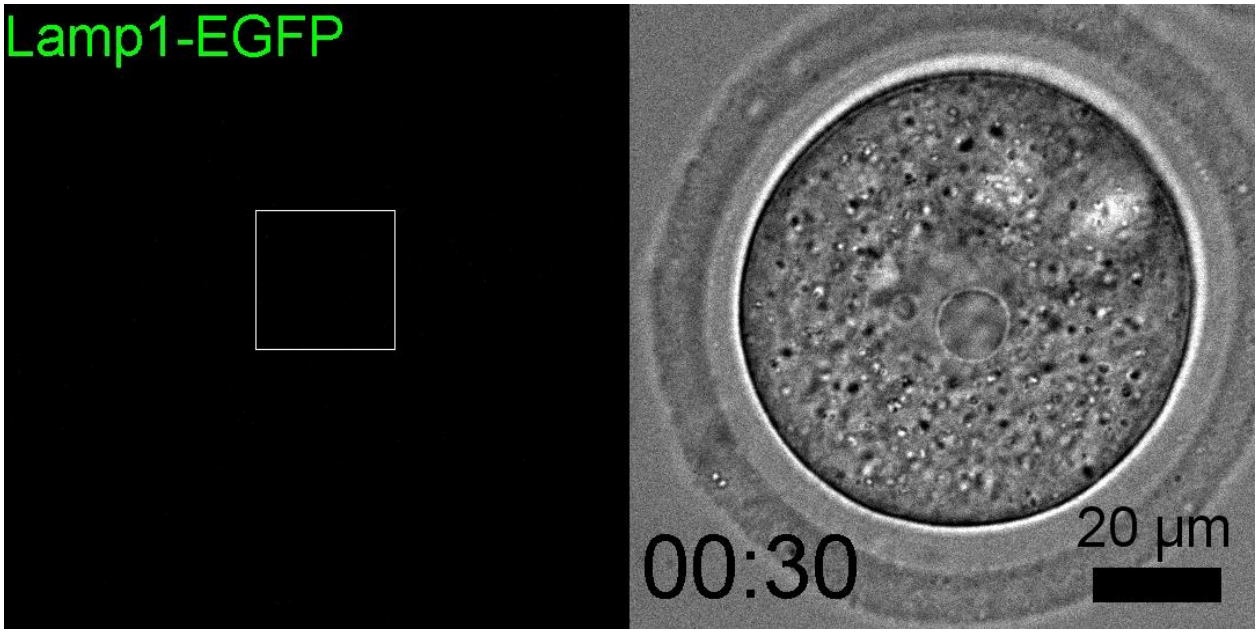

Video 3.
GV oocytes were injected with the mixture mRNA solution for *Lamp1-EGFP* and *V1A-mCherry*, and incubated for IVM. Time-lapse movie of EGFP fluorescence of a representative oocyte is indicated as maximum intensity projection of confocal images with a height of 80 μm. Magnified perinuclear regions in Fig. 5 are indicated by a box. The timestamp indicates the time after IVM started

Video 4

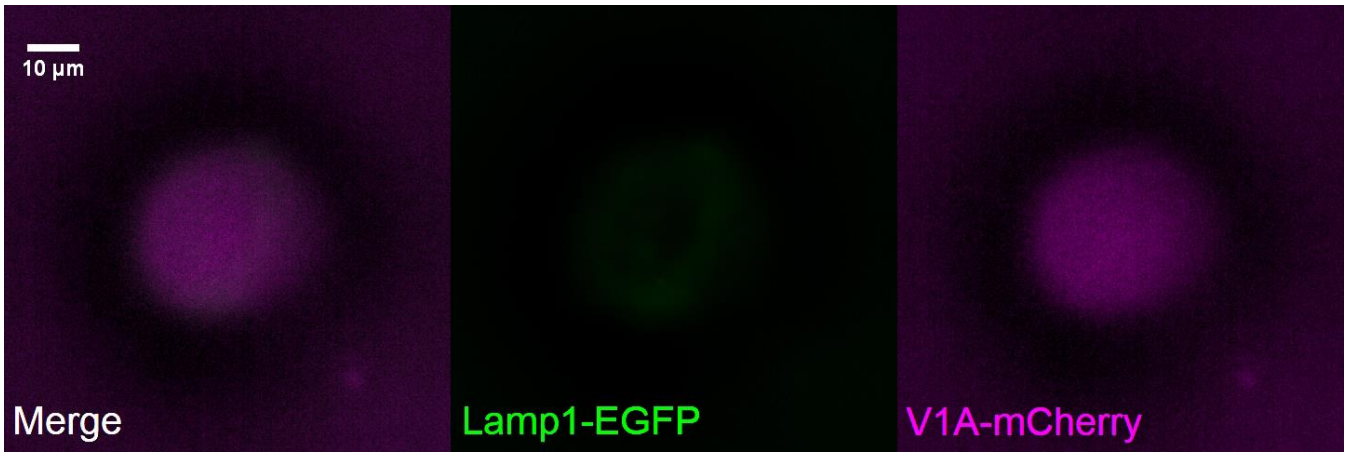

Video 4
GV oocytes were injected with V1A-mCherry mRNA and incubated for 18 h for IVM in the presence of LysoSensor green. Fluorescent images of a representative oocyte which matured to MII stage is presented. A series of the confocal images of 81 slices with a height of 80 µm is shown from top to bottom.

Video 5

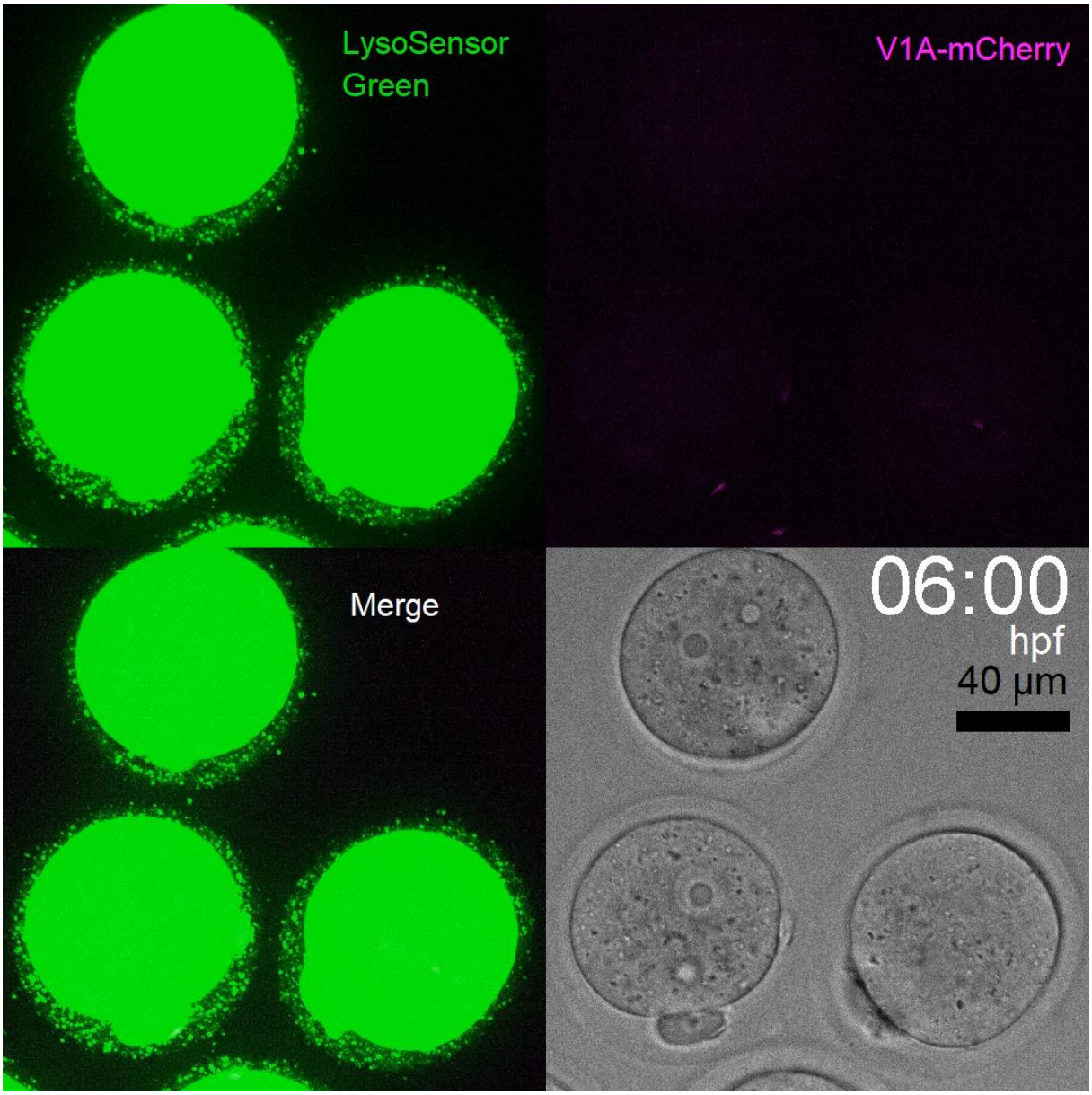

Video 5.
Embryos were injected with V1A-mCherry mRNA at 3 hpf and incubated for further embryogenesis in the presence of LysoSensor Green during embryonic development. A time-lapse movie of a representative embryo is shown (maximum intensity projection of confocal images at a height of 80 µm).